Evaluation of Small Tail Probabilities Directly from the Characteristic Function

Albert H. Nuttall
Surface Undersea Warfare Directorate

19971021 036

DTIC QUALITY INSPECTED 4

Naval Undersea Warfare Center Division
Newport, Rhode Island
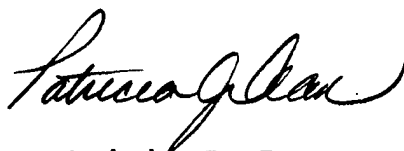
PREFACE

The work described in this report was sponsored by the Independent Research Program of the Naval Undersea Warfare Center Division, Newport, RI, under Project No. B100077, "Near-Optimum Detection of Random Signals with Unknown Locations, Structure, Extent, and Strengths," principal investigator Albert H. Nuttall (Code 311). The independent research program is funded by the Office of Naval Research; the Naval Undersea Warfare Center Division Newport program manager is Stuart C. Dickinson (Code 102).

The technical reviewer for this report was Paul M. Baggenstoss (Code 2121).

Reviewed and Approved: 15 September 1997

Patricia J. Dean

Patricia J. Dean
Director, Surface Undersea Warfare

REPORT DOCUMENTATION PAGE

Form Approved
OMB No. 0704-0188

Public reporting burden for this collection of information is estimated to average 1 hour per response, including the time for reviewing instructions, searching existing data sources, gathering and maintaining the data needed, and completing and reviewing the collection of information. Send comments regarding this burden estimate or any other aspect of this collection of information, including suggestions for reducing this burden, to Washington Headquarters Services, Directorate for Information Operations and Reports, 1215 Jefferson Davis Highway, Suite 1204, Arlington, VA 22202-4302, and to the Office of Management and Budget, Paperwork Reduction Project (0704-0188), Washington, DC 20503.

1. AGENCY USE ONLY *(Leave blank)*	2. REPORT DATE 15 September 1997	3. REPORT TYPE AND DATES COVERED Progress

4. TITLE AND SUBTITLE Evaluation of Small Tail Probabilities Directly from the Characteristic Function	5. FUNDING NUMBERS PE 0601152N

6. AUTHOR(S)

Albert H. Nuttall

7. PERFORMING ORGANIZATION NAME(S) AND ADDRESS(ES) Naval Undersea Warfare Center Division 1176 Howell Street Newport, Rhode Island 02841-1708	8. PERFORMING ORGANIZATION REPORT NUMBER NUWC-NPT TR 10,840

9. SPONSORING/MONITORING AGENCY NAME(S) AND ADDRESS(ES) Office of Naval Research 800 North Quincy Street, BCT 1 Arlington, VA 22217-5000	10. SPONSORING/MONITORING AGENCY REPORT NUMBER

11. SUPPLEMENTARY NOTES

12a. DISTRIBUTION/AVAILABILITY STATEMENT Approved for public release; distribution is unlimited.	12b. DISTRIBUTION CODE

13. ABSTRACT *(Maximum 200 words)*

An efficient, fast, and accurate Fourier transform technique for obtaining small tail probabilities for both the probability density function and the exceedance distribution function, directly from the characteristic function, is derived and demonstrated numerically for several examples. The method is especially useful when analytic or asymptotic expressions for the probabilities are unavailable or unknown.

By choosing the shift parameter r close to the highest singularity of the characteristic function in the complex plane, very small values of the tail probabilities of the density function and exceedance distribution function can be realized. The cost in this approach is that the sampling increment must then be taken small, in order to avoid aliasing. Finer sampling necessitates more computer time and effort, but it does not require more storage;

14. SUBJECT TERMS Tail Probabilities Characteristic Function Probability Density Exceedance Distribution Fast Fourier Transform Aliasing			15. NUMBER OF PAGES 54
			16. PRICE CODE

17. SECURITY CLASSIFICATION OF REPORT Unclassified	18. SECURITY CLASSIFICATION OF THIS PAGE Unclassified	19. SECURITY CLASSIFICATION OF ABSTRACT Unclassified	20. LIMITATION OF ABSTRACT SAR

NSN 7540-01-280-5500

Standard Form 298 (Rev. 2-89)
Prescribed by ANSI Std Z39-18

rather, prealiasing can be advantageously employed to keep the fast Fourier transform size at reasonable values. The fast Fourier transform size has no effect upon the errors caused by aliasing and truncation; rather, the size merely controls the spacing at which the probability density function and exceedance distribution function outputs are calculated. Tail probabilities in the E-50 range are readily available with a computer limited to 15 significant decimal digits.

TABLE OF CONTENTS

LIST OF ILLUSTRATIONS

LIST OF ABBREVIATIONS AND SYMBOLS

a_n	Real part of location of a singularity
b_n	Imaginary part of location of a singularity
b_1	Minimum imaginary part of singularity locations
c	Additive real constant
C	Contour of integration, equation (17)
CF	Characteristic function, equation (1)
EDF	Exceedance distribution function, equation (17)
$E(u)$	Exceedance distribution function of x, equation (17)
$\underline{E}(u)$	Auxiliary function, equation (19)
$\tilde{E}(u)$	Periodic function, equation (21)
$f(\xi)$	Characteristic function of x, equation (1)
$f_+(\xi)$	Characteristic function of positive-u part of p(u)
$f_-(\xi)$	Characteristic function of negative-u part of p(u)
$\tilde{f}_m$	Finite sequence of samples, equation (12)
FFT	Fast Fourier transform, equation (13)
Im	Imaginary part, equation (2)
N	Size of FFT, equation (13)
N_f	Integer in the noise region, equation (25)
PDF	Probability density function, equation (1)
Prob	Probability
$p(u)$	Probability density function of x, equation (1)
$\underline{p}(u)$	Auxiliary function, equation (6)
$\tilde{p}(u)$	Periodic function, equation (7)
r	Real shift in path of ξ integration, equation (4)
Re	Real part, equations (9), (10), (21)

LIST OF ABBREVIATIONS AND SYMBOLS (Cont'd)

u_n General sampling point, equation (15)

x Random variable

Δ_u Increment in u, equation (14)

Δ_x Sampling increment, equations (7), (21)

ε_m Weighting sequence, equations (10), (21)

bold   Random variable

EVALUATION OF SMALL TAIL PROBABILITIES
DIRECTLY FROM THE CHARACTERISTIC FUNCTION

INTRODUCTION

Given the characteristic function (CF) $f(\xi)$ of a random variable x, the corresponding probability density function (PDF) $p(u)$ can be found analytically by the Fourier transform

$$p(u) = \frac{1}{2\pi} \int_{-\infty}^{\infty} d\xi \, \exp(-iu\xi) \, f(\xi) \ . \tag{1}$$

The CF $f(\xi)$ exists for all real ξ because the area under nonnegative PDF $p(u)$ is unity. However, when integral (1) cannot be accomplished in closed form, it is often necessary to resort to a numerical technique, namely, the fast Fourier transform (FFT) to obtain approximate values of PDF $p(u)$.

Similarly, the exceedance distribution function (EDF), $E(u) = \text{Prob}(x > u) = \int_{u}^{\infty} dt \, p(t)$, corresponding to CF $f(\xi)$, is available by the Fourier transform (reference 1, equation (4.14) or reference 2, page 3)

$$E(u) = \frac{1}{2} + \frac{1}{\pi} \int_{0}^{\infty} \frac{d\xi}{\xi} \, \text{Im}\left(f(\xi) \, \exp(-iu\xi)\right) \ . \tag{2}$$

If this latter integral (2) cannot be done in closed form, or if the indefinite integral of PDF $p(u)$ is unavailable, an efficient

numerical technique employing the FFT can again be utilized (references 2 through 4).

However, there is an inherent limitation in the numerical approximations to integrals (1) and (2) in their current forms, as integrals along the real ξ-axis. Both require sampling and summing integrands with values in the neighborhood of unity and relying on the cancellation of complex plus-and-minus values (contributed by the oscillating exponential $\exp(-iu\xi)$) to reach very small values on the tails of the PDF $p(u)$ or EDF $E(u)$ for large u. If the computer being used is limited to D significant decimal digits, then the small tail probabilities calculated for $p(u)$ or $E(u)$, which are less than approximately 10^{-D}, are useless because these values are buried in the inherent round-off noise.

In this report, an efficient technique for obtaining small tail probabilities, significantly less than 10^{-D}, is presented for both the PDF $p(u)$ and the EDF $E(u)$. The basic idea is to move the contour of integration into the complex ξ-plane; however, care must then be taken to control the aliasing that always accompanies equispaced sampling, which in turn, is required for efficient use of an FFT. Examples of the proposed technique are presented for both the PDF and the EDF. Values of small tail probabilities in the 10^{-50} range are readily achieved using a computer with $D = 15$ significant decimal digits.

2

DEVELOPMENT OF TECHNIQUE FOR PDF

MOVEMENT OF CONTOUR FOR PDF

The CF $f(\xi)$ follows from the PDF $p(u)$ according to the inverse Fourier transform

$$f(\xi) = \int_{-\infty}^{\infty} du \, \exp(i\xi u) \, p(u)$$

$$= \int_{-\infty}^{0} du \, \exp(i\xi u) \, p(u) + \int_{0}^{\infty} du \, \exp(i\xi u) \, p(u) \equiv f_{-}(\xi) + f_{+}(\xi) \, . \quad (3)$$

The component $f_{-}(\xi)$, corresponding to $u \leq 0$, is analytic for $\xi_i < 0$ because $\exp(-\xi_i u)$ is bounded for $u \leq 0$. The decay of $p(u)$ as $u \to -\infty$ is arbitrary.

It is presumed that the PDF $p(u)$ has already been shifted on the u-axis so that it is virtually zero for $u < 0$, yet is packed as closely as possible to the origin at abscissa values near $u = 0+$. This condition can be accomplished by adding a real constant c to the random variable under investigation. Addition of a constant c corresponds to multiplication of the corresponding CF by the factor $\exp(ic\xi)$; this factor is presumed to be present in the given CF $f(\xi)$. The constant c can be positive or negative, depending on the desired direction of shift of a given PDF, so as to make $p(u)$ essentially nonzero only in the positive neighborhood of $u = 0$.

This section focuses on the positive tail of PDF $p(u)$. It is presumed that $p(u)$ decays according to $u^\alpha \exp(-\beta u)$ as $u \to +\infty$, $\beta > 0$. Then, the locations $\xi_n = a_n - i \, b_n$ of all singularities of $f_+(\xi)$ must satisfy $b_n > 0$ for all n. Let $b_1 = \min\{b_n\}$, without loss of generality. Then, $p(u) \exp(ru)$ decays exponentially as $u \to +\infty$, provided that real constant $r < b_1$. Accordingly, the Fourier relation in equation (1) can be written as

$$p(u) = \frac{1}{2\pi} \int_{-\infty-ir}^{\infty-ir} d\xi \, \exp(-iu\xi) \, f(\xi) , \quad 0 < r < b_1 . \tag{4}$$

This path of integration passes through the horizontal strip of analyticity between the real ξ-axis and the highest singularity of $f(\xi)$ in the lower-half ξ-plane.

For example, PDF $p(u) = 1.5 \exp(-u) - \exp(-2u)$, for $u > 0$ has CF $f(\xi) = 1.5/(1-i\xi) - 1/(2-i\xi)$, with poles at $\xi = -i$ and $\xi = -i2$. Thus, $a_1 = 0$, $b_1 = 1$, $a_2 = 0$, $b_2 = 2$, and $r < 1$. As a second example, $p(u) = u \exp(-u)$, for $u > 0$ has $f(\xi) = 1/(1-i\xi)^2$ with $a_1 = 0$, $b_1 = 1$, for which $r < 1$. Finally, Gaussian PDF $p(u) = (2\pi)^{-\frac{1}{2}} \exp[-(u-c)^2/2]$ has CF $f(\xi) = \exp(-\xi^2/2 + ic\xi)$, which has no singularities anywhere in the finite ξ-plane. Then, r can be chosen arbitrarily, positive or negative. (Positive constant c is taken as small as possible, subject to PDF value $p(0)$ being sufficiently small, as discussed earlier.)

4

Upon making the substitution $x = \xi + ir$ in equation (4), it follows that

$$p(u) = \exp(-ru) \, \underline{p}(u) \, , \tag{5}$$

where auxiliary function

$$\underline{p}(u) \equiv \frac{1}{2\pi} \int_{-\infty}^{\infty} dx \, \exp(-iux) \, f(x - ir) \, . \tag{6}$$

The real function $\underline{p}(u)$ is nonnegative for all u, but it may not have unit area. The relations in equations (5) and (6) are exact, even if the path of integration is very close to the highest singularity of $f(x - ir)$ in the lower-half x-plane at $x_1 = a_1 - i(b_1 - r)$.

By writing equation (5) in the form $\underline{p}(u) = p(u) \exp(ru)$, it is seen that the closer r is taken to b_1, the less decay there is in $\underline{p}(u)$ for positive u. This property makes $\underline{p}(u)$ a wider function of u and brings some of the originally very small values of p(u) up to moderate levels; of course, the exponential decay of $\underline{p}(u)$ will eventually take over, but it will be shifted to larger u values before becoming dominant. Thus, larger values of r (nearer b_1) enable investigation of deeper tails of p(u) than possible when r = 0, namely, using the real ξ-axis in equation (4).

Because PDF p(u) $\cong$ 0 for u < 0, the same is true for $\underline{p}(u)$, according to equation (5). Also, the essential nonzero region of

$\underline{p}(u)$ is in the positive neighborhood of $u = 0$.

(If the negative tail of random variable **x** is of interest, consider the variable **y** = T − **x**, for which the PDF is $p_y(u) = p_x(T - u)$. Real constant T is taken just large enough that **y** is essentially nonzero only in the positive neighborhood of zero. Then, the CF of interest is $f_y(\xi) = \exp(i\xi T) \, f_x(-\xi)$ instead of $f_x(\xi)$.)

SAMPLING AND ALIASING FOR PDF

Fourier relation (6) for widened function $\underline{p}(u)$ is evaluated approximately by sampling at increment Δ_x for all x. (Truncation errors are discussed below.) The result is

$$\underline{p}(u) \cong \frac{\Delta_x}{2\pi} \sum_{m=-\infty}^{\infty} \exp(-ium\Delta_x) \, f(m\Delta_x - ir) \equiv \tilde{p}(u) \quad \text{for all } u \; . \quad (7)$$

The latter real function, $\tilde{p}(u)$, is periodic in u, with period $2\pi/\Delta_x$. In fact, it is the aliased version of $\underline{p}(u)$:

$$\tilde{p}(u) = \sum_{m=-\infty}^{\infty} \underline{p}\left(u - m\frac{2\pi}{\Delta_x}\right) \quad \text{for all } u \; . \quad (8)$$

For $\tilde{p}(u)$ to be a good approximation to $\underline{p}(u)$ in the positive neighborhood of $u = 0$, the aliasing lobes of $\tilde{p}(u)$ must be sufficiently separated so that the fundamental period, interval $(0, 2\pi/\Delta_x)$, is only slightly contaminated by the undesired lobes

contributed when $m = \pm 1, \pm 2, \ldots$. (Recall that $\underline{p}(u)$ is essentially nonzero only in the positive neighborhood of $u = 0$.) This requirement can be checked by looking at one period of $\tilde{p}(u)$, namely, $0 < u < 2\pi/\Delta_x$, to determine if the skirts near $u = 0+$ and $u = 2\pi/\Delta_x-$ are sufficiently small. If not, sampling increment Δ_x must be decreased. Then, $\tilde{p}(u)$ will be a good approximation to $\underline{p}(u)$ in the interval $(0, 2\pi/\Delta_x)$.

It should be recalled that the closer r is taken to b_1, the less decay there is in $\underline{p}(u)$ (see equation (5)); that is, $\underline{p}(u)$ is wider in u, leading to more severe aliasing problems in equation (8), unless Δ_x is additionally decreased, separating the lobes of $\tilde{p}(u)$ farther apart. This additional decrease is an unavoidable consequence of investigating deeper tails of $p(u)$ by relations (5) and (6).

The proximity of the path of integration in equation (6) to the nearest singularity of $f(x - ir)$ does not require an additional decrease in sampling increment Δ_x; it is all accounted for in the widening effect of $\exp(ru)$ upon $p(u)$ in the function $\underline{p}(u) = \exp(ru) \, p(u)$ and the attendant more stringent alias-suppression requirement in equation (8).

A shortcut for the evaluation of equation (7) is available by taking advantage of the conjugate symmetry of $f(x - ir)$. In particular, from equation (3), it follows that $f(-x - ir) = f^*(x - ir)$. Then, equation (6) can be expressed as

$$p(u) = \frac{1}{\pi} \, \text{Re} \int_0^\infty dx \, \exp(-iux) \, f(x - ir) \, , \tag{9}$$

and equation (7) can be expressed as

$$p(u) \cong \frac{\Delta_x}{\pi} \, \text{Re} \sum_{m=0}^\infty \varepsilon_m \, \exp(-ium\Delta_x) \, f(m\Delta_x - ir) = \tilde{p}(u) \, . \tag{10}$$

This function is the same function $\tilde{p}(u)$ encountered in equation (7). The sequence $\{\varepsilon_m\}$ is ½ for $m = 0$, and 1 otherwise.

FFT CONSIDERATIONS FOR PDF

Periodic function $\tilde{p}(u)$, defined by equation (7), needs to be evaluated over one period only. In particular, because the function of interest, $p(u)$, is essentially nonzero only in the positive neighborhood of $u = 0$, attention is confined to values

$$\tilde{p}\left(\frac{2\pi}{\Delta_x} \frac{n}{N}\right) = \frac{\Delta_x}{2\pi} \sum_{m=-\infty}^\infty \exp(-i2\pi mn/N) \, f(m\Delta_x - ir) \quad \text{for } 0 \le n \le N-1. \tag{11}$$

However, because the exponential factor $\exp(-i2\pi mn/N)$ treats all complex samples $f(\{m + kN\}\Delta_x - ir)$ equally, regardless of the value of integer k, these samples can be collapsed (or prealiased) into a set of just N values according to

$$\tilde{f}_m \equiv \sum_{k=-\infty}^\infty f\left((m + kN)\Delta_x - ir\right) \quad \text{for } 0 \le m \le N-1 \, . \tag{12}$$

This process accounts for all the samples of f encountered in equation (11). FFT size N can be much smaller than the number of terms required in equation (12) to control and minimize truncation errors. Then, equation (11) can be written exactly as finite sum

$$\tilde{p}\left(\frac{2\pi}{\Delta_x}\frac{n}{N}\right) = \frac{\Delta_x}{2\pi}\sum_{m=0}^{N-1}\exp(-i2\pi mn/N)\,\tilde{f}_m \quad \text{for } 0 \leq n \leq N-1 \;. \quad (13)$$

Because the N infinite sums required by equation (12) can never be conducted in practice, it is necessary to truncate them where $|f(x - ir)|$ is sufficiently small. The effect of the resultant truncation errors can be observed in the u domain as a low-level oscillatory behavior when equation (13) is plotted. If this level is excessive, a smaller tolerance must be set on truncating equation (12), and additional values for larger $|k|$ must be taken into account.

Operation (13) can be accurately and efficiently realized as an N-point FFT if N is taken as a power of 2. Observe that FFT size N does not affect the truncation error or the aliasing error; rather, N merely sets the spacing in variable u in equation (13), namely,

$$\Delta_u = \frac{2\pi}{N\Delta_x}\;, \quad (14)$$

at which output $\tilde{p}(u)$ is obtained.

PLOTTING PROCEDURE

It is recommended that output (13) be plotted over the full sweep of n values and observed for its near-origin behavior, aliasing, and truncation errors. Then, additive constant c, or sampling increment Δ_x, or the truncation limits in equation (12), or any combination of the three can be modified, and the entire procedure repeated until all errors are acceptable. Also, regions of u where $\tilde{p}(u)$ is below the inherent round-off error of the computer will appear with a white-noise strip of low-level values; this white-noise strip gives a measure of the relative errors of the values obtained for $\tilde{p}(u)$ in the _entire_ region $0 < u < 2\pi/\Delta_x$.

If the following points in the fundamental interval are defined according to

$$u_n = n\ \Delta_u = \frac{2\pi}{\Delta_x}\frac{n}{N} \quad \text{for } 0 \leq n \leq N-1 \ , \tag{15}$$

then, the desired values of pdf p(u) are available from equations (5), (7), and (13) according to

$$p(u_n) = \exp(-ru_n)\ \underline{p}(u_n) \cong \exp(-ru_n)\ \tilde{p}(u_n)$$

$$= \exp(-ru_n)\ \frac{\Delta_x}{2\pi}\sum_{m=0}^{N-1}\exp(-i2\pi mn/N)\ \tilde{f}_m \quad \text{for } 0 \leq n \leq N-1 \ . \tag{16}$$

A plot of this approximation to p(u), in conjunction with the relative error information obtained from the earlier plot of $\tilde{p}$ in

equation (13), reveals the levels of PDF p(u) and the relative errors associated with different regions of u. If the lowest levels reached by equation (16) are not sufficiently small, parameter r in equations (4) and (12) must be increased and the plots of equations (13) and (16) must be repeated. As noted earlier, doing so will likely entail a decrease in sampling increment Δ_x to control aliasing of a wider $\underline{p}(u)$. A short trial-and-error procedure may be required.

MOVEMENT OF CONTOUR FOR EDF

The Fourier transform relating the EDF $E(u) = \text{Prob}(x > u)$ to the CF $f(\xi)$ can be written in the form

$$E(u) = \int_{u}^{\infty} dt\, p(t) = \frac{1}{i2\pi} \int_{C} d\xi\, \frac{f(\xi)}{\xi} \exp(-iu\xi) \, , \qquad (17)$$

where contour C is the real ξ-axis, except that it passes below the singularity at $\xi = 0$. The comments regarding the corresponding PDF $p(u)$ in equation (3) and sequel are directly relevant to equation (17). In particular, as in equation (4), the contour is moved to distance r below the real ξ-axis, where real constant r is less than the distance to the nearest singularity of $f(\xi)$ in the lower-half ξ-plane to obtain

$$E(u) = \frac{1}{i2\pi} \int_{-\infty-ir}^{\infty-ir} d\xi\, \frac{f(\xi)}{\xi} \exp(-iu\xi) = \exp(-ru)\, \underline{E}(u) \, , \qquad (18)$$

where auxiliary function

$$\underline{E}(u) \equiv \frac{1}{i2\pi} \int_{-\infty}^{\infty} dx\, \frac{f(x - ir)}{x - ir} \exp(-iux) \, . \qquad (19)$$

Here, the substitution $x = \xi + ir$ was used. Relation (19) is still a Fourier transform, although with a modified integrand.

The real function $\underline{E}(u)$ is nonnegative for all u. Relations (18) and (19) are exact, even if the path of integration is very close to the highest singularity of f(x − ir) in the lower-half x-plane at $x_1 = a_1 - i(b_1 - r)$, $b_1 > 0$.

By writing equation (18) in the form $\underline{E}(u) = E(u) \exp(ru)$, it is seen that the closer r is taken to b_1, the less decay there is in $\underline{E}(u)$ for positive u. For u > 0, $\underline{E}(u)$ becomes a wider function of u and brings some of the originally very small values of E(u) up to moderate levels; of course, the exponential decay of $\underline{E}(u)$ as u → +∞ eventually takes over, but it is shifted to larger u values before becoming dominant. Thus, larger values of r (nearer b_1) enable investigation of deeper tails of E(u) than possible when r = 0, namely, using the real ξ-axis in equation (17).

The dominant asymptotic behaviors of functions E(u) and $\underline{E}(u)$ are as follows:

$$E(u) \propto \begin{cases} 1 & \text{as } u \to -\infty \\ \exp(-b_1 u) & \text{as } u \to +\infty \end{cases} \quad , \quad \underline{E}(u) \propto \begin{cases} \exp(ru) & \text{as } u \to -\infty \\ \exp(ru - b_1 u) & \text{as } u \to +\infty \end{cases}.$$

$$(20)$$

By taking $0 < r < b_1$, $\underline{E}(u)$ decays to zero for both u → ±∞. Taking r close to b_1 keeps $\underline{E}(u)$ at a high level (near $\underline{E}(0)$) for an extended range of positive u. It also gives maximum decay to the left tail of $\underline{E}(u)$, which will be seen to be advantageous in terms of alias control. If $\underline{E}(u)$ can be accurately calculated for

large positive u, then relation (18) will result in accurate evaluation of E(u) at very low levels of probability.

It is important to observe that, unlike the original EDF E(u), the modified EDF $\underline{E}(u)$ decays to zero as $u \to \pm\infty$; the original EDF E(u) always approaches 1 as $u \to -\infty$. This feature of $\underline{E}(u)$ allows the integral of equation (19) to be approximated by a sampling procedure and yet have controllable aliasing lobes.

SAMPLING AND ALIASING FOR EDF

Fourier relation (19) for modified EDF $\underline{E}(u)$ is evaluated approximately by sampling at increment Δ_x for all x. The result is

$$\underline{E}(u) = \frac{1}{\pi} \text{Re} \int_0^\infty dx \; \frac{f(x - ir)}{r + ix} \; \exp(-iux) =$$

$$\cong \frac{\Delta_x}{\pi} \text{Re} \sum_{m=0}^\infty \varepsilon_m \; \frac{f(m\Delta_x - ir)}{r + im\Delta_x} \; \exp(-ium\Delta_x) \equiv \tilde{E}(u) \quad \text{for all u . (21)}$$

The latter real function, $\tilde{E}(u)$, is periodic in u, with period $2\pi/\Delta_x$; in fact, it is the aliased version of $\underline{E}(u)$:

$$\tilde{E}(u) = \sum_{m=-\infty}^\infty \underline{E}\left(u - m \frac{2\pi}{\Delta_x}\right) \quad \text{for all u .} \qquad (22)$$

For $\tilde{E}(u)$ to be a good approximation to $\underline{E}(u)$ in the positive neighborhood of u = 0, the aliasing lobes of $\tilde{E}(u)$ must be

15

sufficiently separated so that the fundamental period, interval
$(0,2\pi/\Delta_x)$, is only slightly contaminated by the undesired lobes
contributed when m = ±1,±2,.... (Recall that $\underline{E}(u)$ is essentially
nonzero only in the neighborhood of u = 0; see equation (20).)
This aliasing requirement can be checked by looking at one period
of $\tilde{E}(u)$, namely, $0 < u < 2\pi/\Delta_x$, to see if the skirts near u = 0+
and $u = 2\pi/\Delta_x$- are sufficiently small. If they are not, sampling
increment Δ_x must be decreased. Then, $\tilde{E}(u)$ can be made a good
approximation to $\underline{E}(u)$ in an interval of length $(0,2\pi/\Delta_x)$ located
about u = 0.

From equations (18) and (21), interest is centered on

$$E(u) = \exp(-ru)\ \underline{E}(u) \cong \exp(-ru)\ \tilde{E}(u) \tag{23}$$

for u in the fundamental period of length $2\pi/\Delta_x$ in the
neighborhood of zero. Accurate results for EDF E(u) are obtained
when $\tilde{E}(u)$ has experienced insignificant aliasing, which is
accomplished by choosing Δ_x small enough. Because $\underline{E}(u)$ for u > 0
has purposely been stretched out over a wider u interval, by
choice of r, Δ_x must be made quite small. Making Δ_x quite small,
however, is an inherent requirement for investigating very low
levels of E(u) because these low levels are not realized until a
considerable interval of u has been covered. In other words, the
more stringent requirement on Δ_x is not due to the particular
procedure, but rather, due to the desire to investigate a wider
range of positive u values, namely, those including very small

E(u). That procedure naturally requires a larger spacing of the aliasing lobes of $\tilde{E}(u)$ to clear out a wider interval of u space so that the ever-present aliasing does not become intolerable.

FFT CONSIDERATIONS FOR EDF

Because $\tilde{E}(u)$ has period $2\pi/\Delta_x$, its evaluation can be limited to one period. In particular, consider

$$\tilde{E}\left(\frac{2\pi}{\Delta_x}\frac{n}{N}\right) = \frac{\Delta_x}{\pi} \operatorname{Re} \sum_{m=0}^{\infty} \varepsilon_m \frac{f(m\Delta_x - ir)}{r + im\Delta_x} \exp(-i2\pi mn/N) \text{ for } 0 \le n \le N-1.$$

$$(24)$$

Presuming that sampling increment Δ_x is taken small enough to effectively eliminate aliasing, a plot of this complete period of $\tilde{E}(u)$ reveals an <u>interior</u> region where the computer round-off noise is dominant.

If an integer in this noise region is defined as N_f, then the values of equation (24) in the range $(0, N_f)$ can be used directly to get estimates of the desired EDF according to

$$E\left(\frac{2\pi}{\Delta_x}\frac{n}{N}\right) = \exp\left(-r\frac{2\pi}{\Delta_x}\frac{n}{N}\right) \underline{E}\left(\frac{2\pi}{\Delta_x}\frac{n}{N}\right) \cong \exp\left(-r\frac{2\pi}{\Delta_x}\frac{n}{N}\right) \tilde{E}\left(\frac{2\pi}{\Delta_x}\frac{n}{N}\right) \quad (25)$$

for $0 \le n \le N_f$. However, the values in the region $N_f < n$ must be scaled differently because they should represent the negative region of E(u) just below the origin, that is, u < 0. The

correct scaling in this region is

$$\exp\left(r \frac{2\pi}{\Delta_x} - r \frac{2\pi}{\Delta_x} \frac{n}{N}\right) \tilde{E}\left(\frac{2\pi}{\Delta_x} \frac{n}{N}\right) \quad \text{for } N_f < n < N \, . \tag{26}$$

These scaled values are typically stored back in bins $N_f < n < N$ and plotted at the upper end of the interval $(0, 2\pi/\Delta_x)$. However, this upper end of the plot must be recognized as the estimate of EDF $E(u)$ just to the left of the origin, that is, $u < 0$. Usually, only the values for $0 \leq n \leq N_f$ are of interest because they encompass the small tail probability values of $E(u)$.

The infinite sum on m in equation (24) must be truncated where the magnitude of complex ratio $f(m\Delta_x - ir)/(r + im\Delta_x)$ becomes insignificant. Values of this complex ratio for $m \geq N$ are simply additively prealiased into bin m MODULO N, thereby avoiding truncation error. Notice that FFT size N has no effect on accuracy; it merely controls the spacing $\Delta_u = 2\pi/(N\Delta_x)$ of output values in equations (24) and (25).

18

EXAMPLES

Four different characteristic functions are considered in this section. For each CF $f(\xi)$, the corresponding PDF $p(u)$ is calculated and plotted, along with an error estimate. In the second half of this section, the corresponding EDFs $E(u)$ are evaluated, in addition to an error estimate. Deeper tail probabilities than considered in these examples are possible through larger choices of the shift parameter r. All the FFT sizes were taken at N = 1024 in this section.

CHI-SQUARE PDF

The CF of interest is $f(\xi) = (1 - i\xi)^{-10}$, which corresponds to a random variable x that is composed of a sum of 20 independent, squared Gaussian random variables with zero mean and common variance ½. Because $x \geq 0$, additive constant c is taken as zero.

Consider, first, the standard FFT approach (1) on this CF, that is, with shift parameter r = 0. The resultant PDF $p(u)$ is displayed in figure 1, where sampling increment $\Delta_x = 2\pi/80$ was used in equation (7) and sequel. The PDF $p(u)$ decays until it reaches the inherent round-off noise of the computer, which is roughly E-15 relative error (64-bit representations). Lower probability (density) estimates are not possible for this example with this standard FFT approach. The maximum abscissa (period) on this plot is $2\pi/\Delta_x$, which is 80 for the above choice of Δ_x.
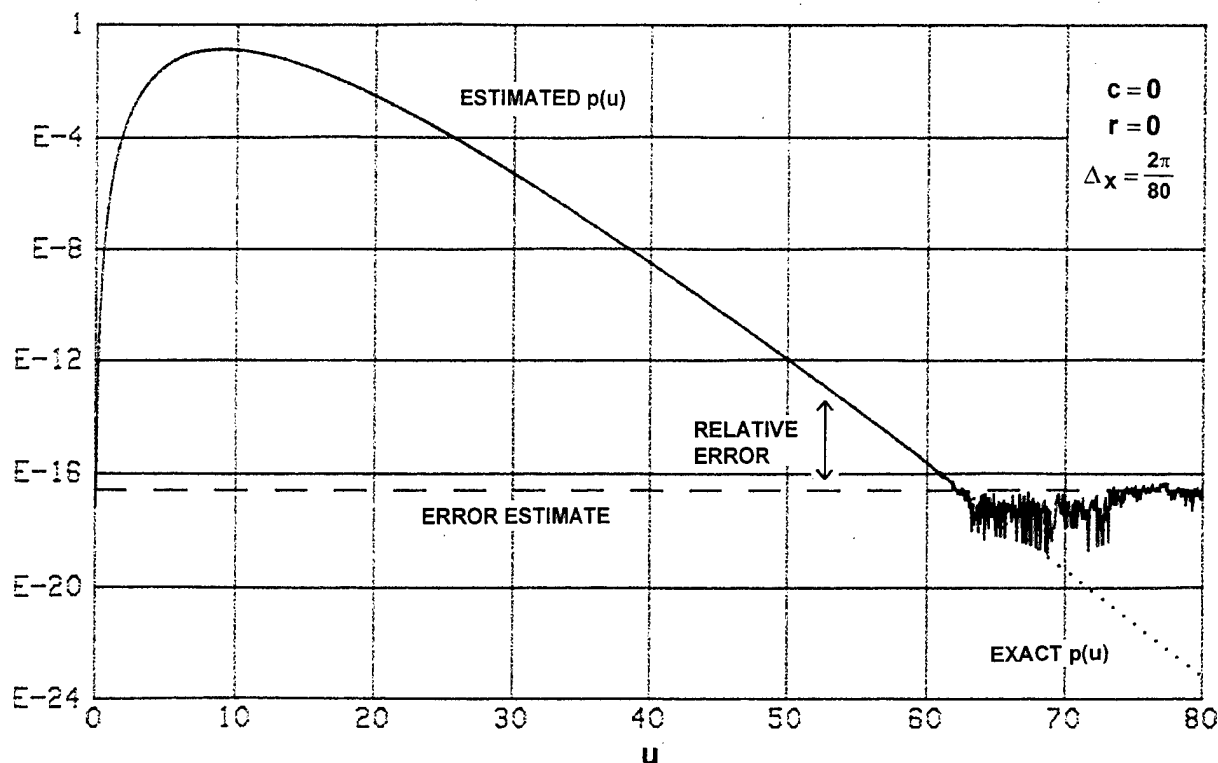
Figure 1. Chi-Square p(u) via Standard FFT Technique

Observe that p(u) drops from E-6 to E-16 in a span of values from u = 32 to u = 61, that is, a span of 29 in u. To reach probability (density) level E-76, for example, an additional span of approximately 6 * 29 = 174 in u is required. To avoid aliasing, a new sampling increment satisfying 61 + 174 = $2\pi/\Delta_x$, namely, $\Delta_x = 2\pi/235$, is required. That is, a noise-free computer would have required $\Delta_x = 2\pi/235$ to get to level E-76 by the standard technique with r = 0.

On the other hand, using shift parameter value r = 0.7, along with c = 0 and Δ_x = 2π/240, the periodic function $\tilde{p}(u)$, defined in equation (7), is presented in figure 2. Naturally, $\tilde{p}(u)$ has a relative error about E-15; furthermore, this small sampling increment Δ_x is observed to be necessary to avoid aliasing at the right tail of $\tilde{p}(u)$.

When the results for $\tilde{p}(u)$ are used in equation (16), the resultant estimate for the desired PDF p(u) is as shown in figure 3. The superposed dashed line is an error estimate, starting from E-12 near the top left and going to the noisy region at the bottom right end. The relative error of the estimated p(u) varies over the range of u values, gradually deteriorating to useless values for u > 200. However, approximately six significant decimal digits are still available at the E-50 probability level. For this example, the exact PDF p(u) is available and has also been plotted in figure 3; it overlies the estimated PDF until the probability values drop below E-75.

GAUSSIAN PDF

The normalized Gaussian CF is $f(\xi) = \exp(-\xi^2/2 + ic\xi)$, where additive constant c is taken as 2. With shift r = 7 and sampling increment Δ_x = 2π/20, the periodic function $\tilde{p}(u)$ is as displayed in figure 4. The sampling increment could not have been taken much smaller without incurring aliasing. Also, the constant c is at its minimum value, just keeping positive values at u = 0+.

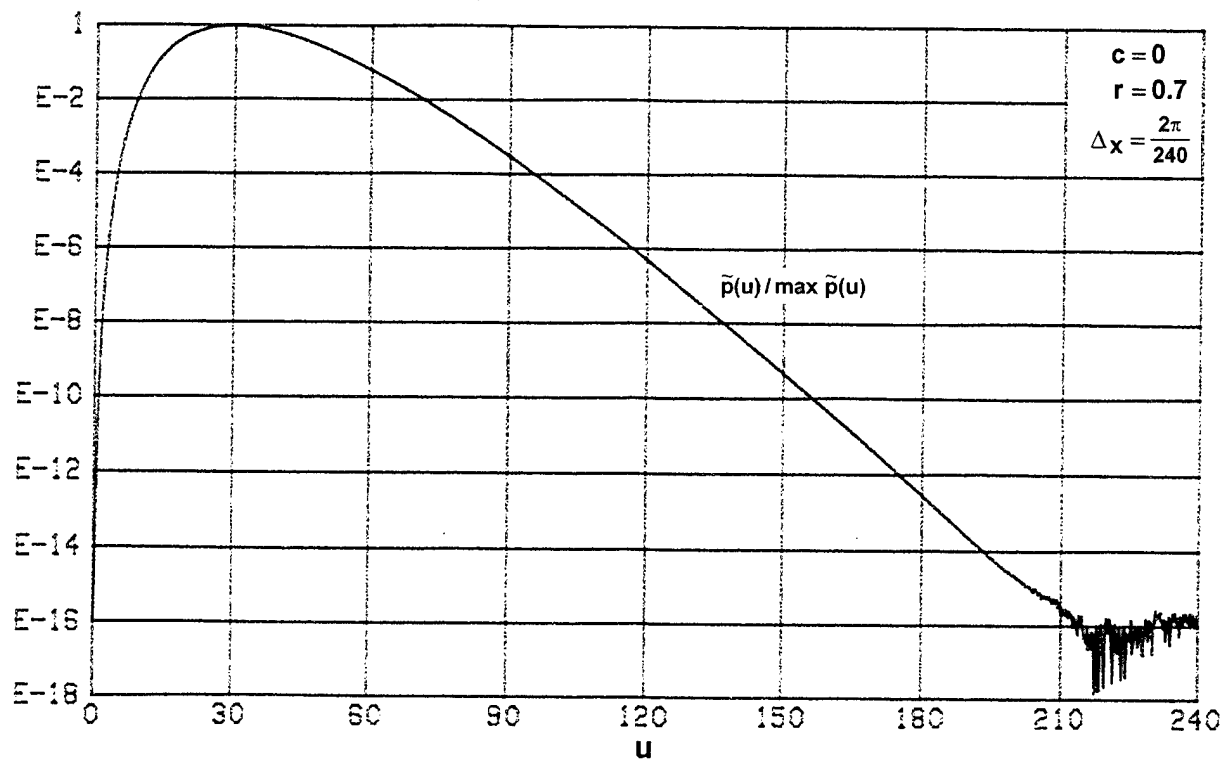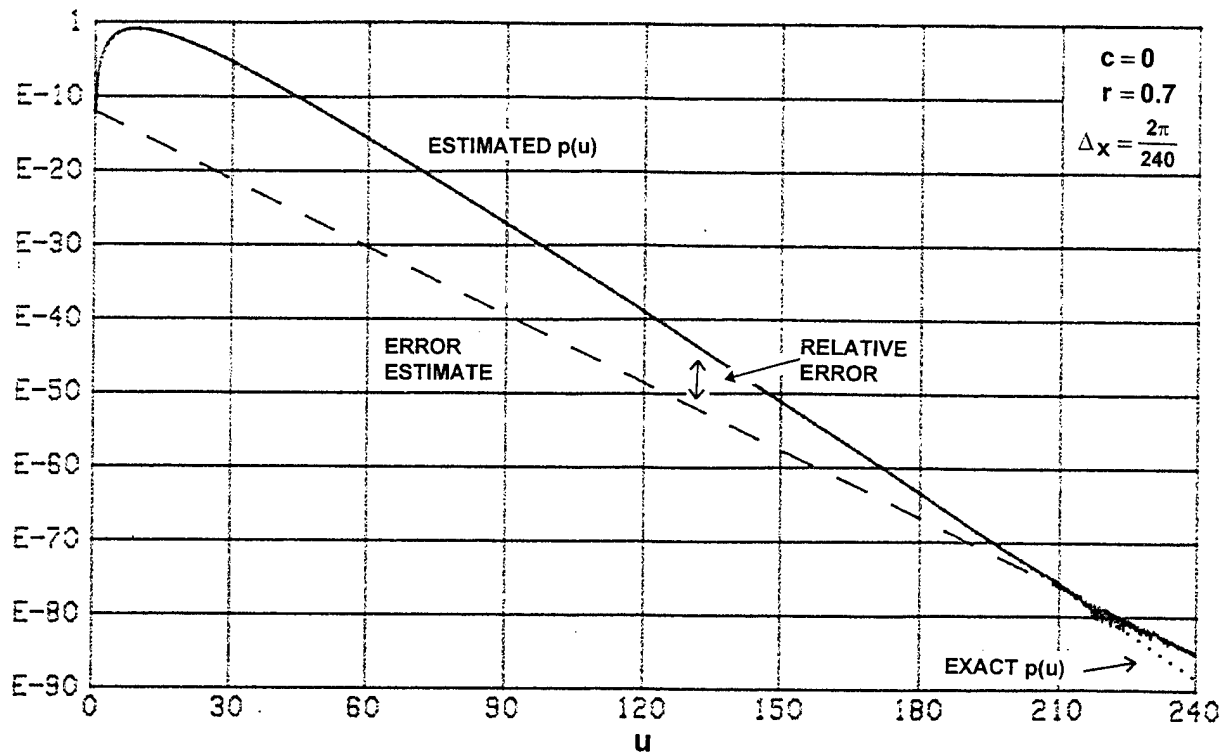Figure 2.   Chi–Square $\tilde{p}(u)$

Figure 3.   Chi–Square $p(u)$

22

The corresponding estimated PDF p(u) is plotted in figure 5, along with the estimated error. The estimated error line joins the two noisy regions at each end of the interval (0,20), which are easily located in $\tilde{p}(u)$ in figure 4. For this example, there are approximately seven decimals of accuracy at the E-40 probability level. The exact PDF p(u) overlies the estimated PDF except at the edges of the interval (0,20); this type of result is again anticipated by the plot of figure 4.

BRANCH POINT PDF

The CF for this example has multiple branch points, namely,

$$f(\xi) = \prod_{n=1}^{10} (1 - i\xi/n)^{-\frac{1}{2}} . \tag{27}$$

This CF corresponds to the sum of 10 independent, squared zero-mean Gaussian random variables with different variances, 1/(2n). The corresponding PDF p(u) is not available in closed form.

The relatively slow decay of this CF, namely, as $1900/\xi^5$, forces numerous evaluations of equation (27) to be undertaken. In fact, with increment $\Delta_x = 2\pi/200$, over 160,000 complex samples were required until $|f(\xi)|$ became sufficiently small to control the truncation error. Nevertheless, employment of prealiasing operation (12) enabled storage and execution of only an N = 1024 point FFT according to equation (13).
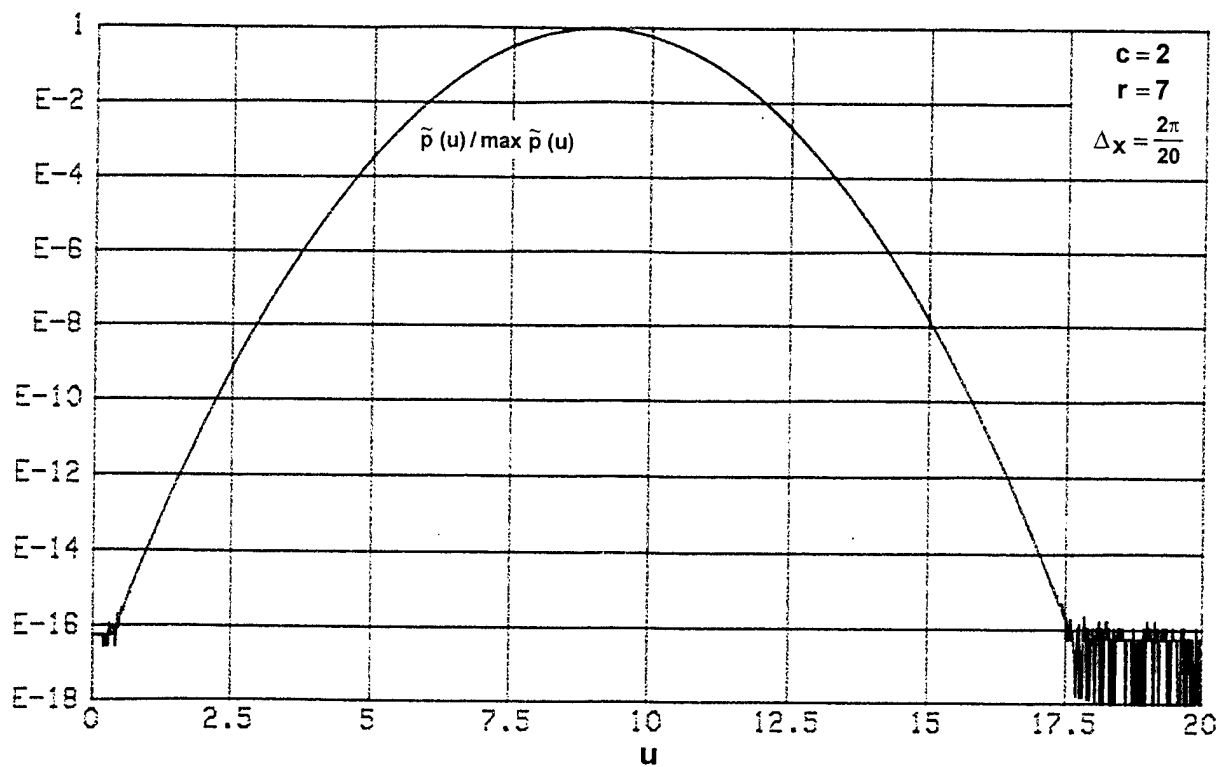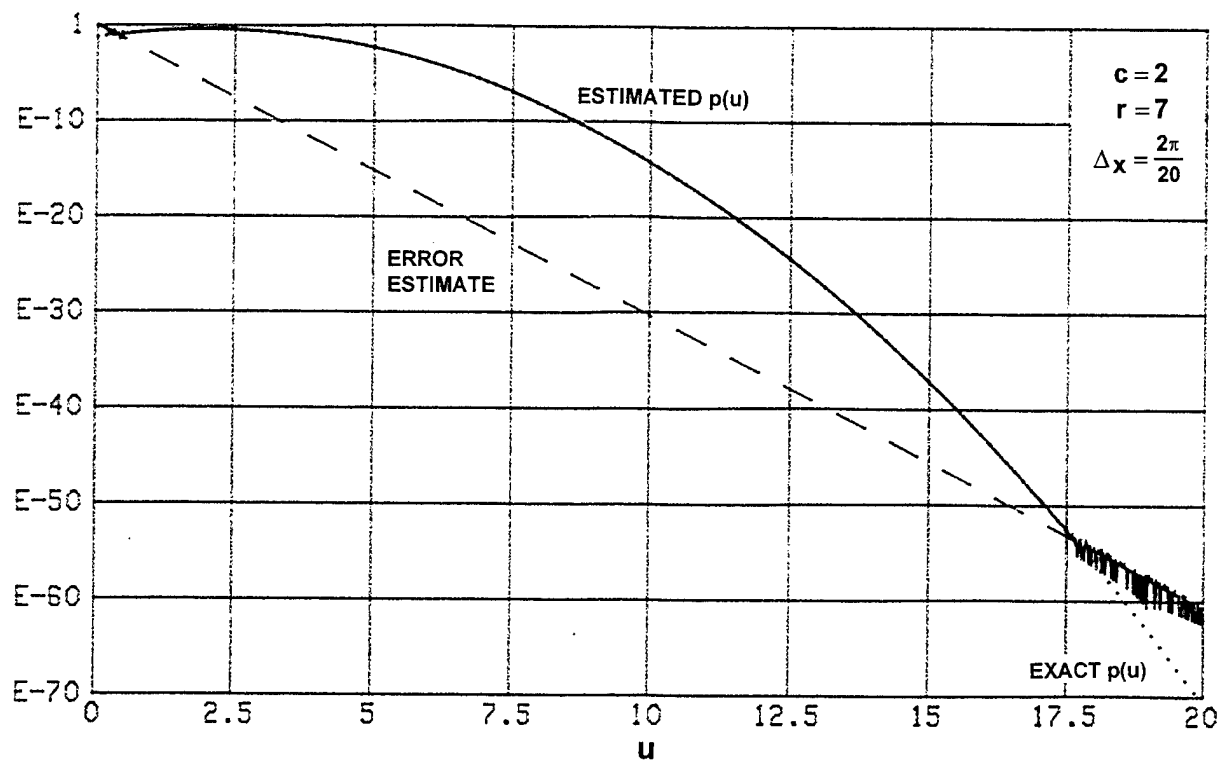
23

Figure 4.   Gaussian $\tilde{p}(u)$

Figure 5.   Gaussian $p(u)$

The function $\tilde{p}(u)$ resulting from operation (13) is displayed in figure 6 for shift $r = 0.8$. The corresponding estimated PDF $p(u)$ is given in figure 7, along with the estimated error. The result for $p(u)$ has approximately six digits of significance at the E-40 probability level.

ESSENTIAL SINGULARITY PDF

The last characteristic function of interest is

$$f(\xi) = \exp\left(i\xi \sum_{n=1}^{10} \frac{1}{1 - i\xi/n}\right) \prod_{n=1}^{10}(1 - i\xi/n)^{-\frac{1}{2}} . \qquad (28)$$

This CF has branch points and essential singularities at $\xi = -in$ and corresponds to a sum of 10 independent, squared Gaussian random variables with a common mean of 1 and different variances $1/(2n)$.

The exponential in equation (28) causes a more rapid decay with ξ; in fact, only 200 samples of the CF were necessary at sampling increment $\Delta_x = 2\pi/200$, using shift $r = 0.6$, to control the truncation error. The resultant $\tilde{p}(u)$, plotted in figure 8, again has relative error in the E-15 range. The corresponding estimated PDF $p(u)$ and its estimated error are displayed in figure 9. There are approximately five digits of significance at the E-40 probability level.
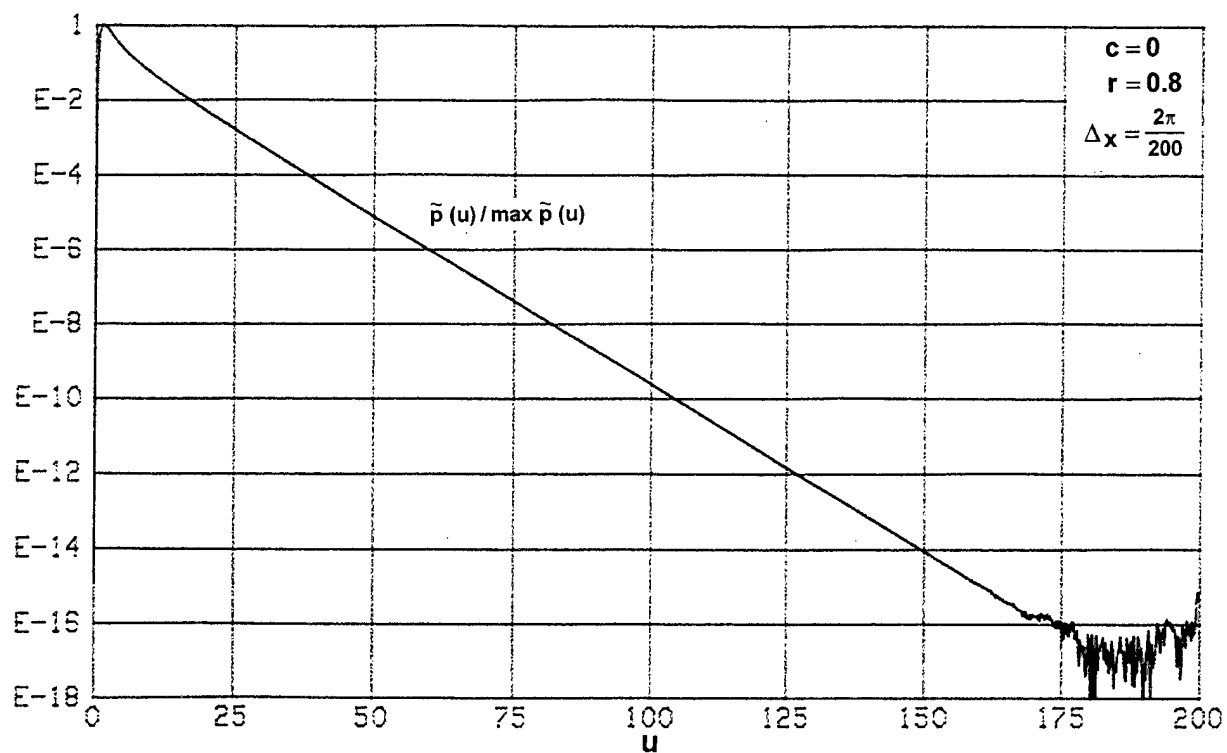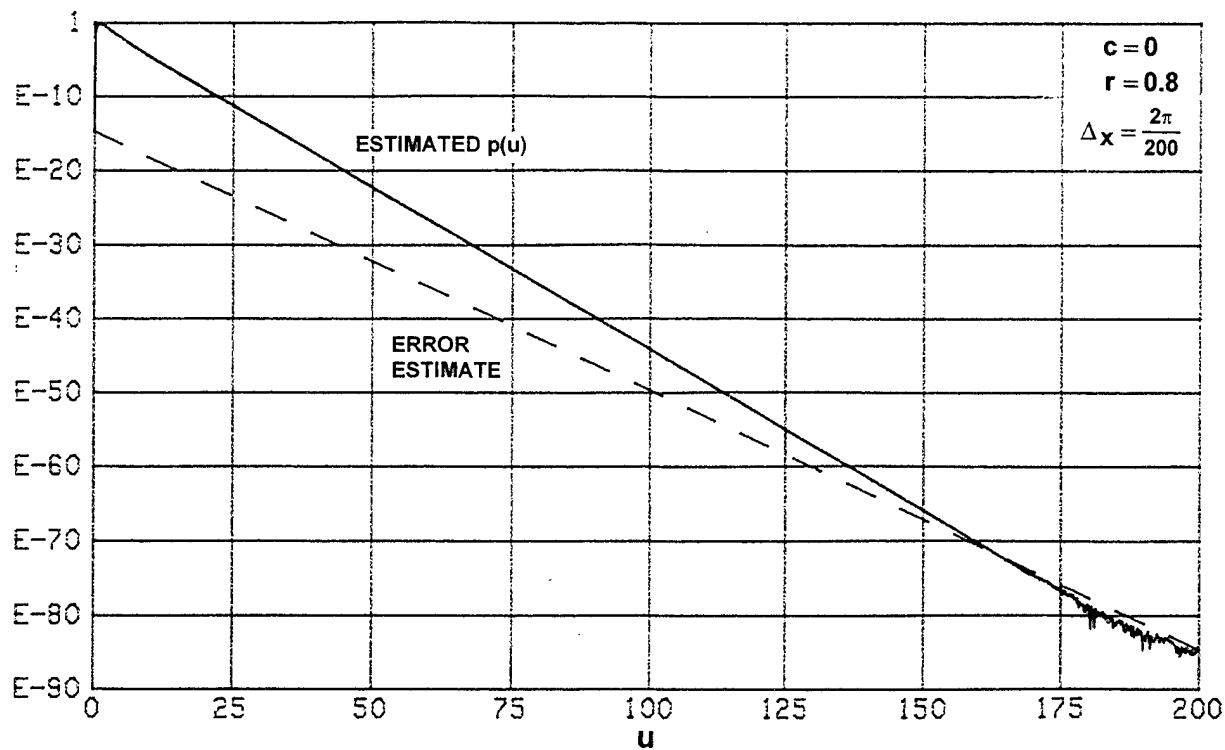
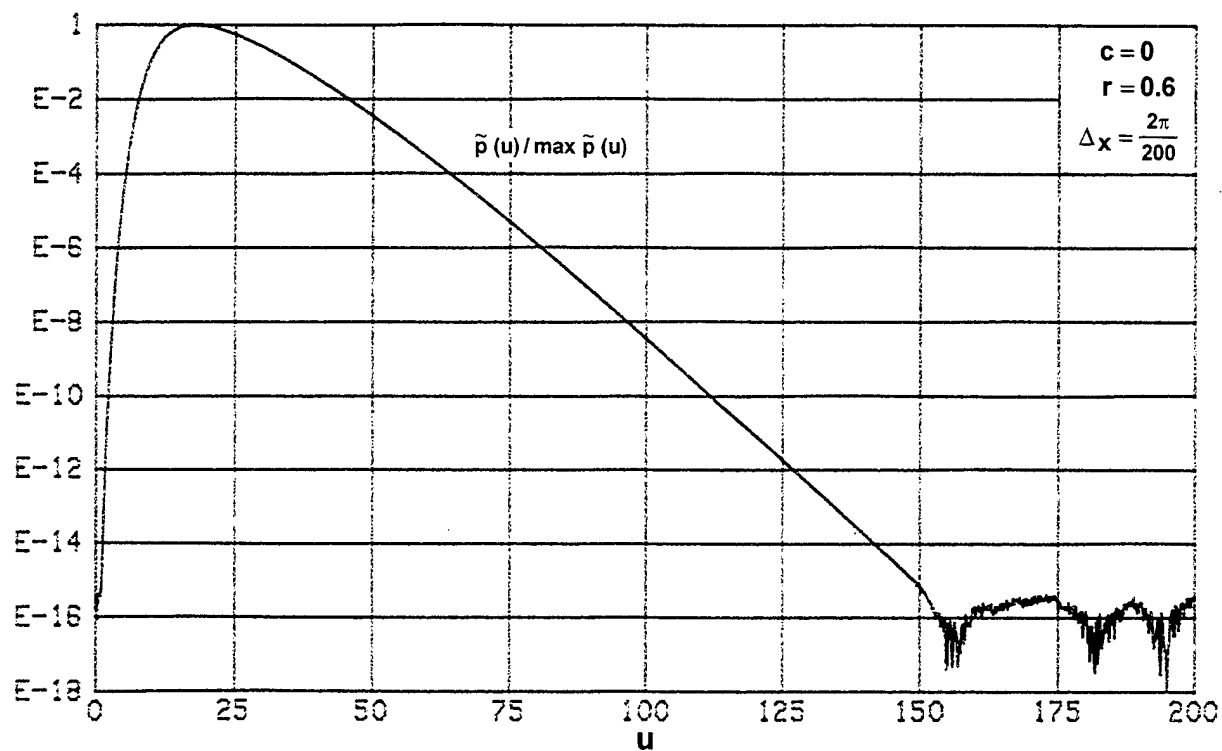Figure 6.   Branch Point $\tilde{p}(u)$

Figure 7.   Branch Point $p(u)$

26

Figure 8. Essential Singularity $\tilde{p}(u)$
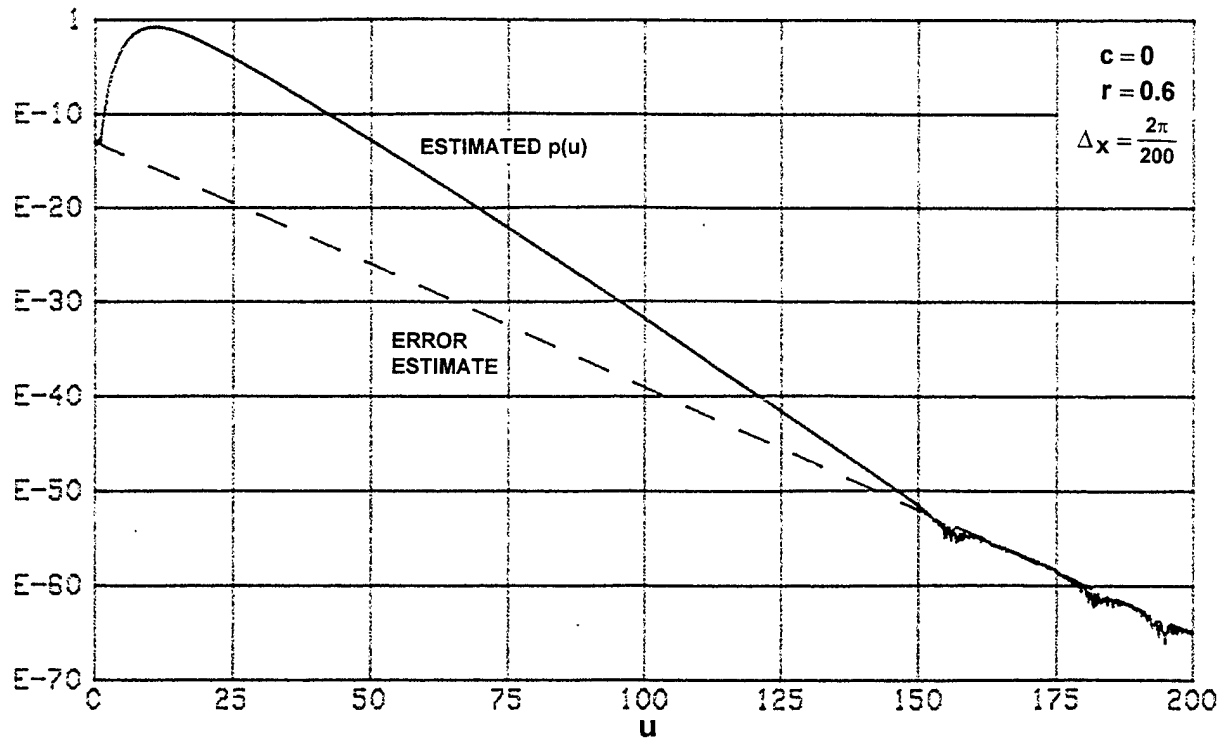
Figure 9. Essential Singularity $p(u)$

27

The CF of interest is again $f(\xi) = (1 - i\xi)^{-10}$. However, for the following examples, the quantity of interest is the EDF E(u). For sampling increment $\Delta_x = 2\pi/240$, shift r = 0.6, and additive constant c = 0, the periodic function $\tilde{E}(u)$ of equations (21) and (24) is presented in figure 10. The nonzero values of $\tilde{E}(u)$ just below u = 240 are the nonzero values of $\underline{E}(u)$ for u < 0 being periodically repeated; this exponential decay of $\underline{E}(u)$, according to equation (20), shows up as a straight line on the logarithmic ordinate. The relative error of $\tilde{E}(u)$ in figure 10 in the noisy region is E-15.

For this example, take the noise-region integer of equation (25) as $N_f = 0.75 \ N = 768$. Then, the estimated EDF E(u), obtained from equations (25) and (26), is presented in figure 11. For u less than 150, the estimated and exact EDFs overlap. Also, for 200 < u < 240, the estimated E(u) recovers its correct value of 1; recall that this region corresponds to u < 0 in the original E(u).

The accuracy of estimated EDF E(u) is about five decimals at the E-40 probability level. The error estimate (dashed line) is obtained by drawing a straight line between the noisy regions established in figure 10; the white-noise level in figure 10 is translated by equations (23) or (25) into a line with slope $-r \log(e) = -0.434 \ r$ on the logarithmic ordinate of figure 11.

Figure 10. Chi-Square $\widetilde{E}(u)$

In this figure: $\widetilde{E}(u)/\max \widetilde{E}(u)$, with $c = 0$, $r = 0.6$, $\Delta_x = \frac{2\pi}{240}$.

Figure 11. Chi-Square $E(u)$

In this figure: ESTIMATED $E(u)$, ERROR ESTIMATE, RELATIVE ERROR, EXACT $E(u)$, with $c = 0$, $r = 0.6$, $\Delta_x = \frac{2\pi}{240}$.

29
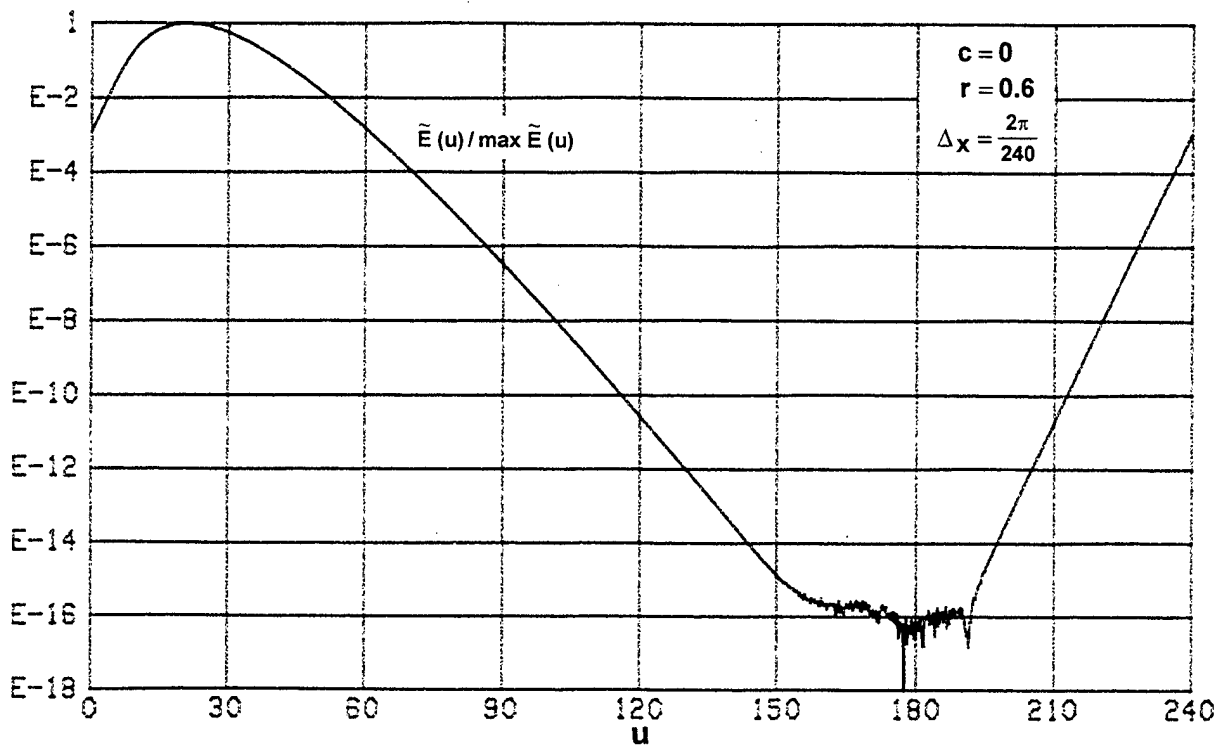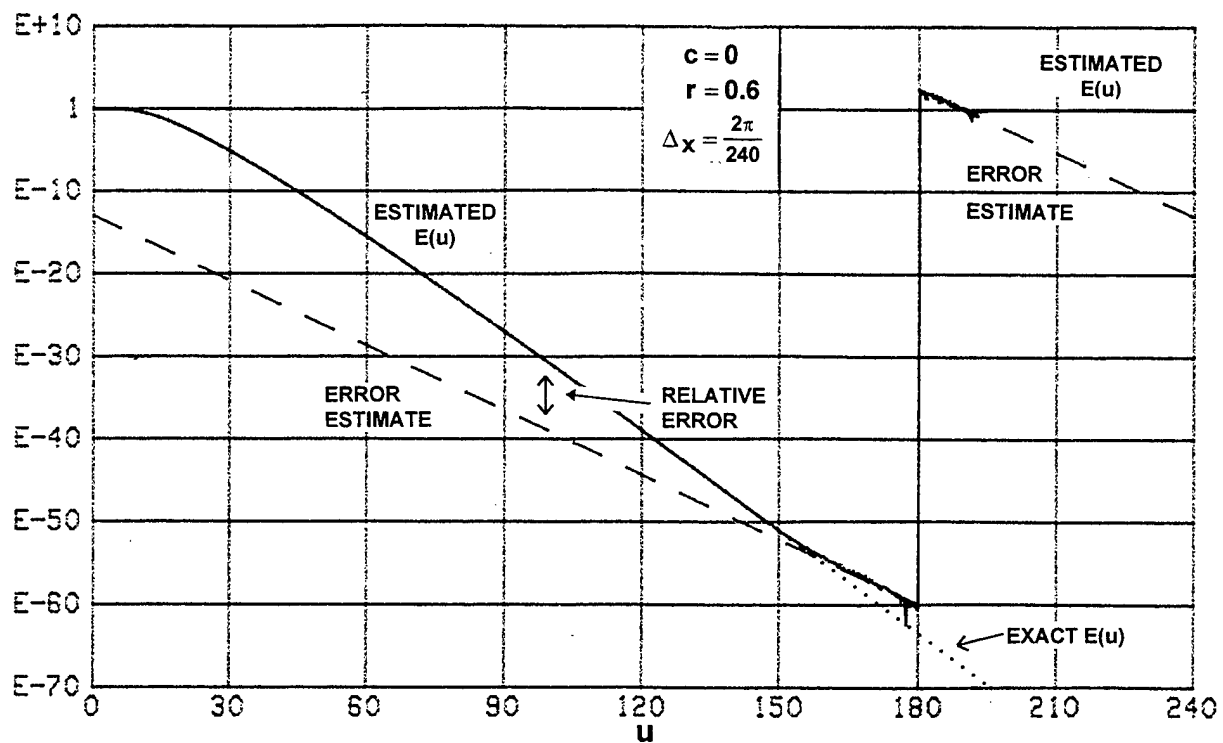
GAUSSIAN EDF

The CF for this example is $f(\xi) = \exp(-\xi^2/2 + ic\xi)$, where constant c is taken as 6. For increment $\Delta_x = 2\pi/24$ and shift r = 5, the periodic function $\tilde{E}(u)$ is as displayed in figure 12. For noise-region integer $N_f = 7/8\ N = 896$, the corresponding estimated E(u) is plotted in figure 13. The stability is approximately six decimals at the E-30 probability level. The estimated E(u) never recovers its unity value for u just less than 24 because the periodic function in figure 12 was not noise-free in that region (in contrast to figures 10 and 11).

BRANCH POINT EDF

The CF $f(\xi)$ was given in equation (27). The increment Δ_x must be taken smaller for the EDF than for the PDF because of the "left" tail of E(u) for u < 0; see equation (20). On the other hand, the number of samples decreased to about 60,000 because of the extra $1/\xi$ decay factor in equations (18) and (21). The periodic function $\tilde{E}(u)$ is given in figure 14. The left tail of E(u) shows up in the region 200 < u < 240.

The corresponding estimated EDF E(u) is displayed in figure 15. It has seven significant digits at the E-40 probability level. The error estimate has slope -0.434 r, which is -0.35 for this example where r = 0.8 has been used.

30
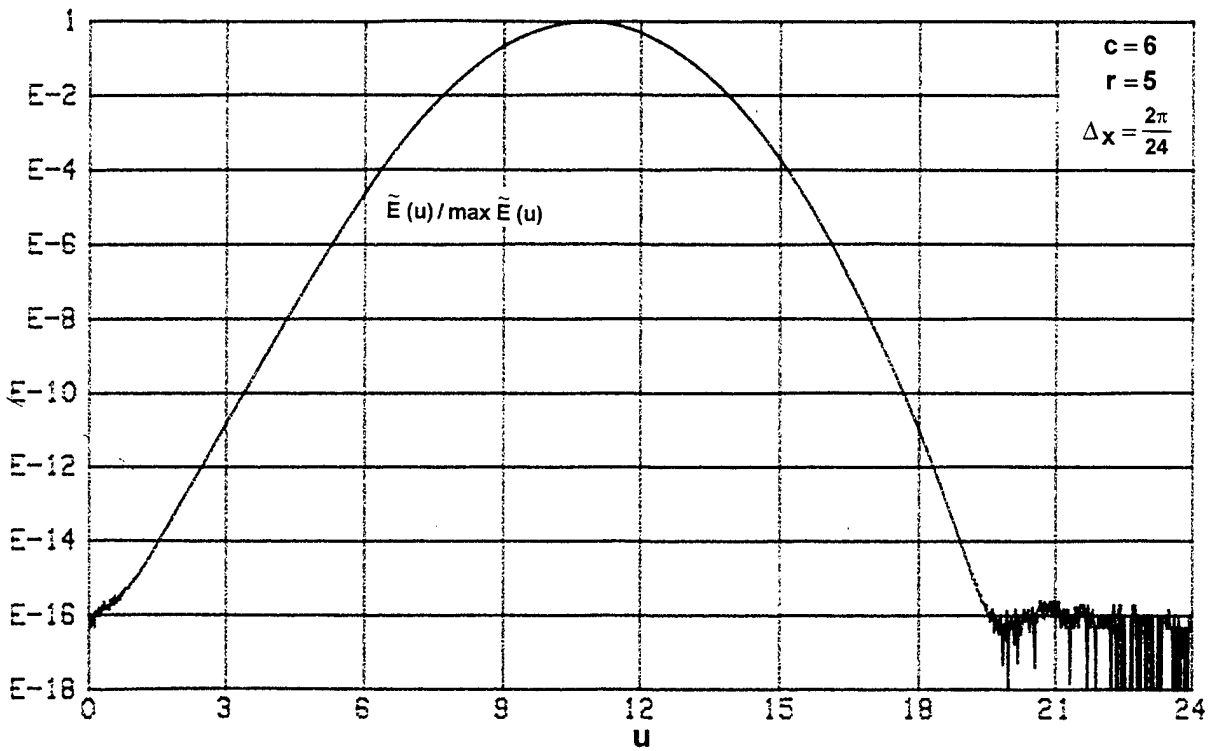
Figure 12.   Gaussian $\tilde{E}(u)$
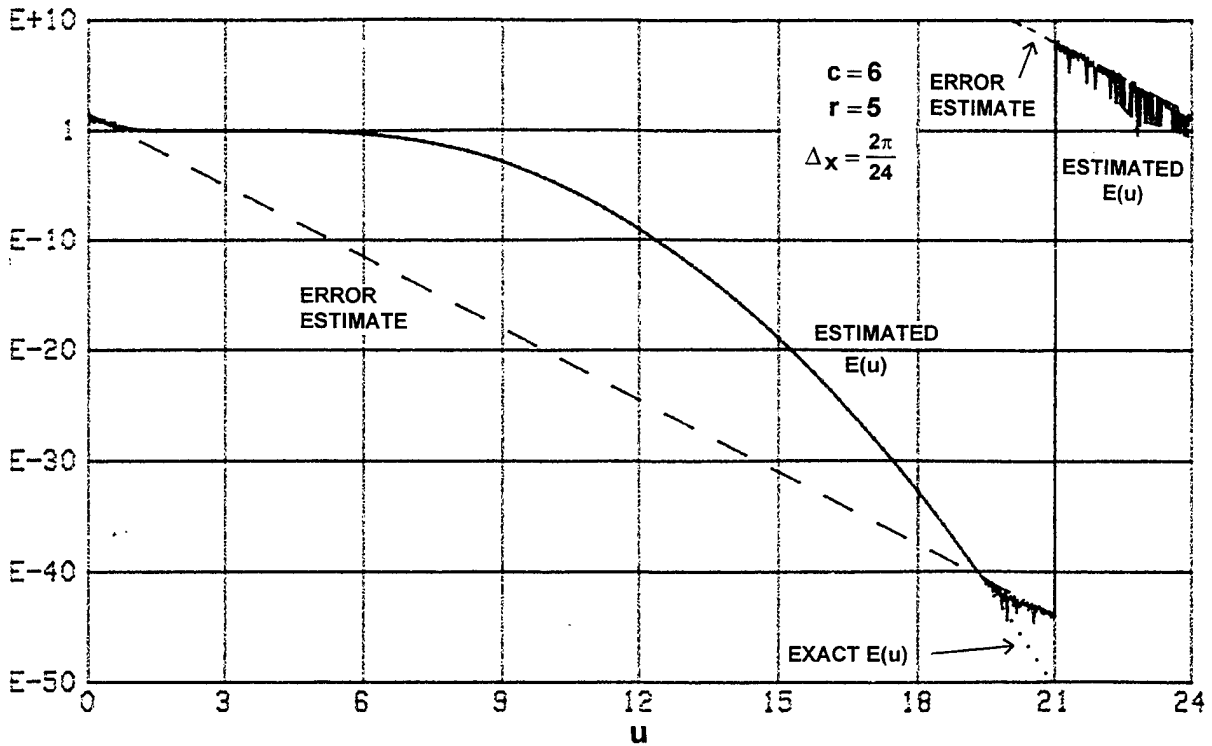
Figure 13.   Gaussian $E(u)$

31
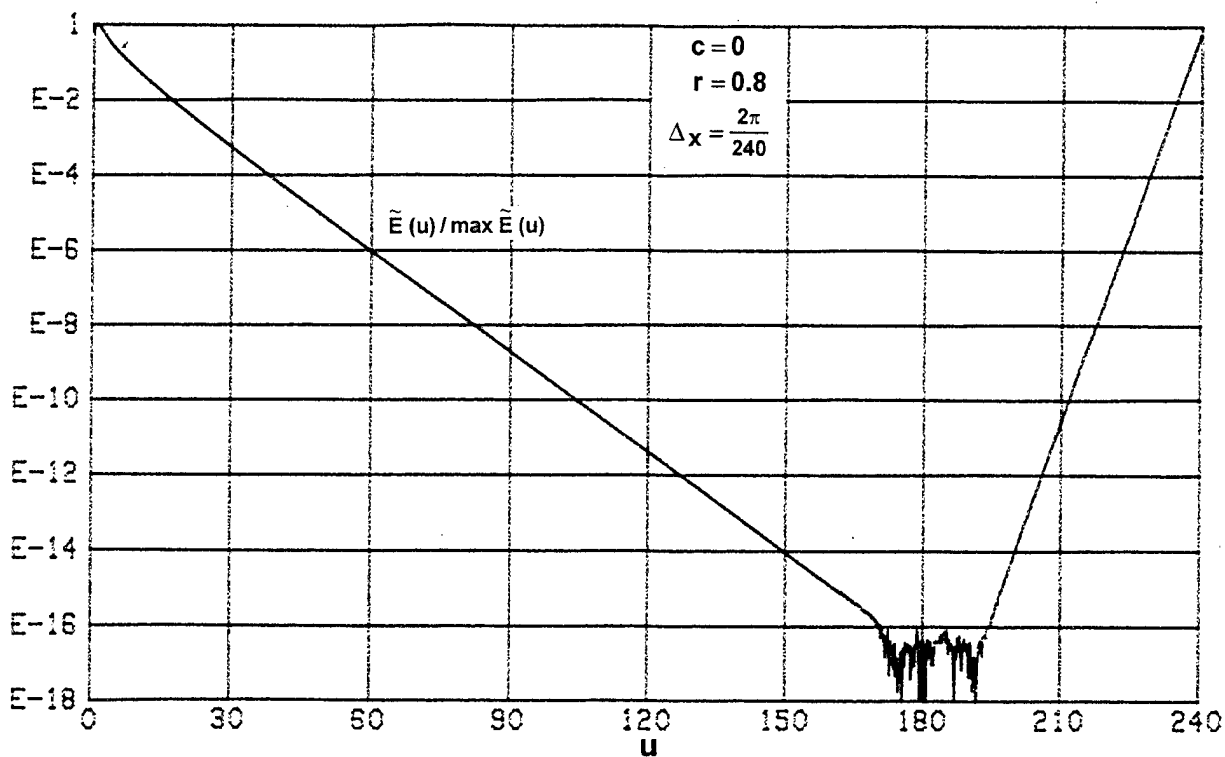
Figure 14. Branch Point $\tilde{E}(u)$
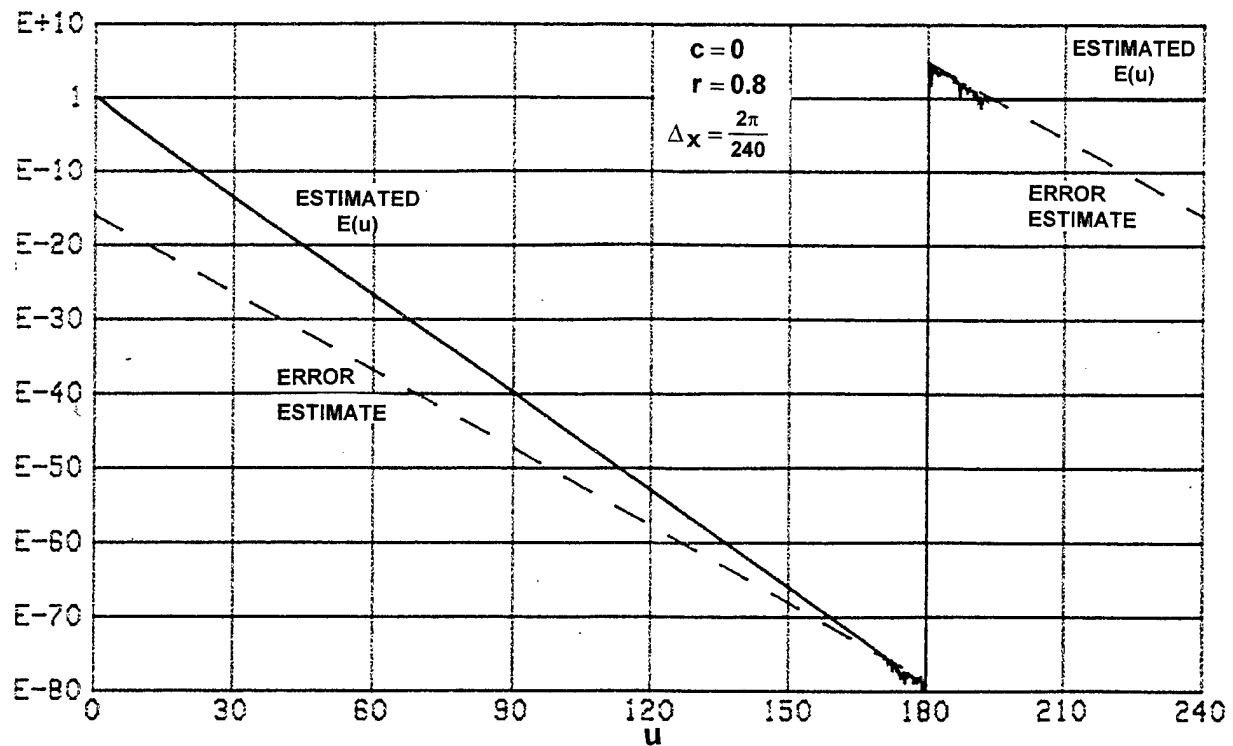
Figure 15. Branch Point $E(u)$

The CF for this example is given by equation (28). The exponential decay of $f(\xi)$ allows accurate calculation of the periodic function $\tilde{E}(u)$ with just over 200 samples of the CF. The left tail in figure 16, just below $u = 240$, is again the periodic repetition of the exponential behavior of $\underline{E}(u)$ for $u < 0$, as indicated in equation (20).

The corresponding estimated EDF $E(u)$ is given in figure 17, along with an error estimate that has a slope of $-0.434 * 0.6 = -0.26$ for $r = 0.6$ in this example. There are approximately four digits of significance in $E(u)$ at the E-40 probability level.
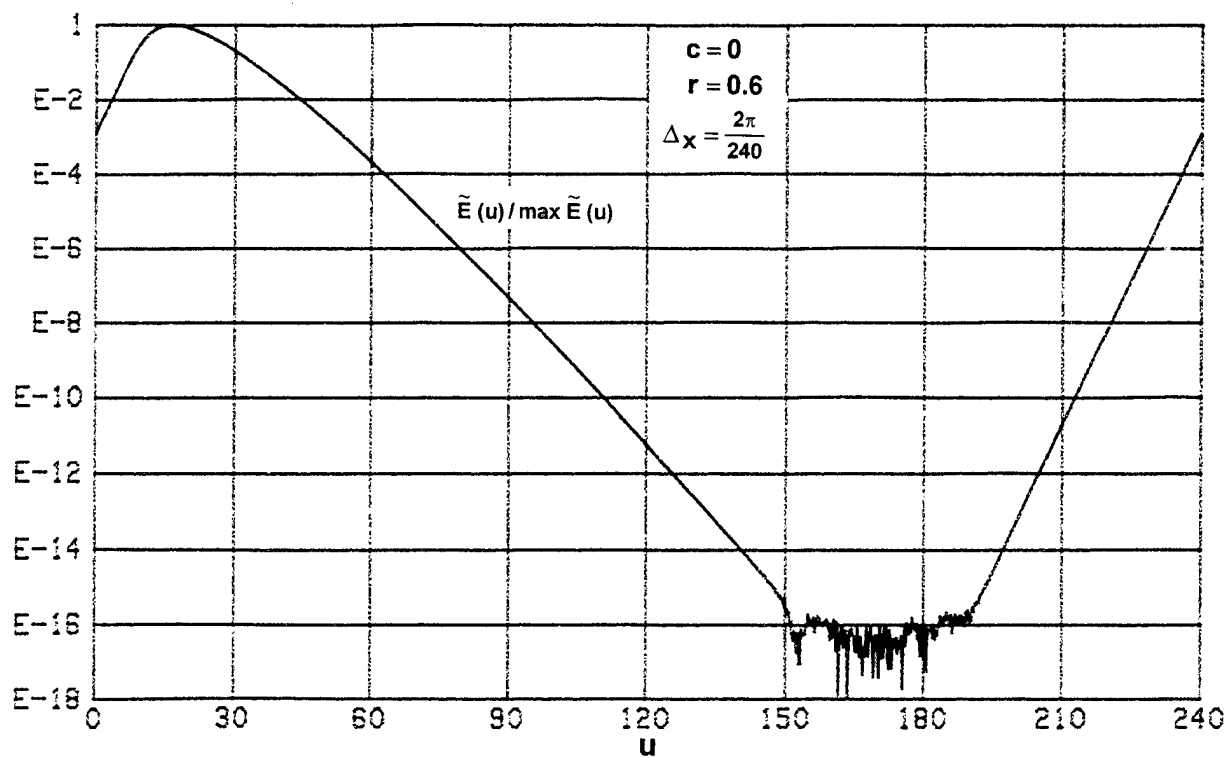
Figure 16.   Essential Singularity $\tilde{E}(u)$
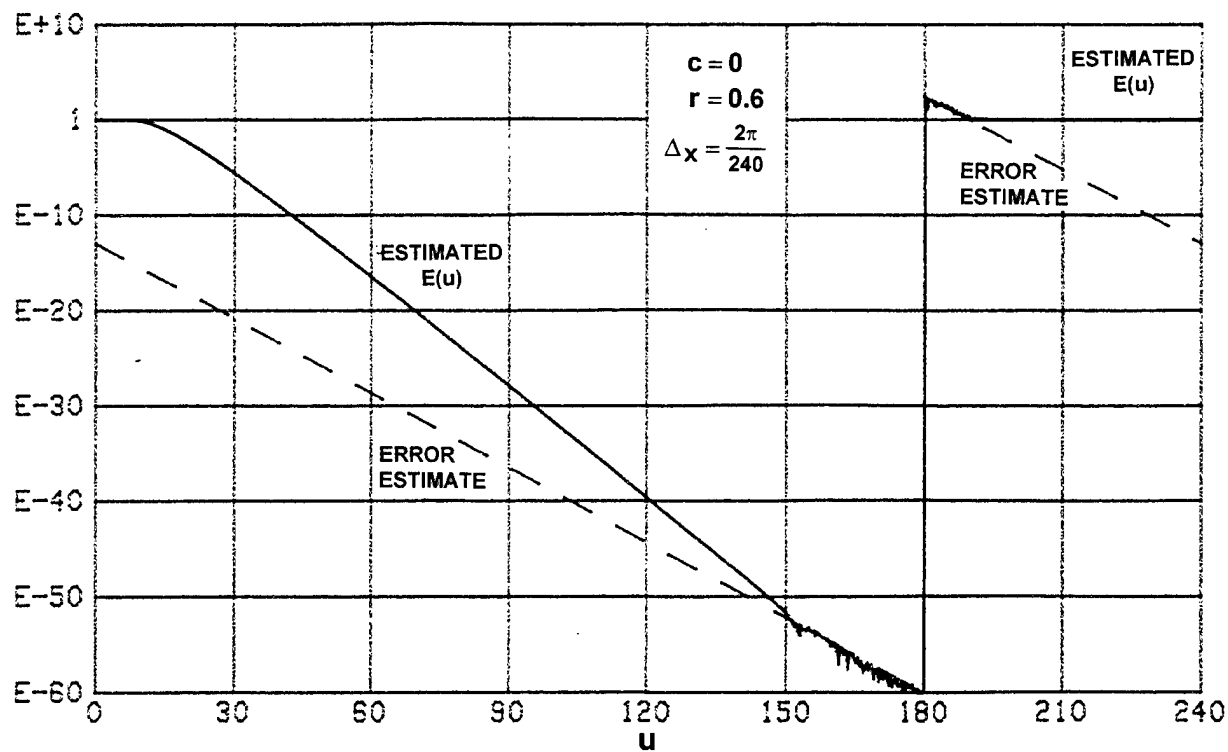
Figure 17.   Essential Singularity E(u)

34

SUMMARY

An efficient, fast, and accurate FFT technique for obtaining small tail probabilities for both the PDF and the EDF, directly from the CF, has been derived and demonstrated numerically for several examples. The method is especially useful when analytic or asymptotic expressions for the probabilities are unavailable or unknown.

By choosing the shift parameter r closer to the highest singularity of CF $f(\xi)$ in the complex ξ-plane, smaller values of the tail probabilities of the PDF and EDF can be realized. The cost in this approach is that the sampling increment Δ_x must then be taken smaller to avoid aliasing. Although taking a smaller Δ_x necessitates more computer time and effort, it does not have to involve more storage because prealiasing can be advantageously employed to keep the FFT size N at very reasonable values. The FFT size N has no effect upon the errors caused by aliasing and truncation; rather, N merely controls the spacing at which the PDF and EDF outputs are calculated.

A sample BASIC program for calculating the PDF $p(u)$ is listed in appendix A, and the corresponding program for the EDF $E(u)$ is given in appendix B. Inputs required of the user are additive constant c, shift r, sampling increment Δ_x, and the particular CF $f(\xi)$. Some trial and error may be necessary in selecting the best values of r and Δ_x.

REFERENCES

1. M. G. Kendall and A. Stuart, **The Advanced Theory of Statistics, Volume 1, Distribution Theory,** Hafner Publishing Company, New York, NY, 1969.

2. A. H. Nuttall, "Accurate Efficient Evaluation of Cumulative or Exceedance Probability Distributions Directly from Characteristic Functions," NUSC Technical Report 7023, Naval Underwater Systems Center, New London, CT, 1 October 1983.

3. A. H. Nuttall, "Numerical Evaluation of Cumulative Probability Distribution Functions Directly from Characteristic Functions," **Proceedings of the Institute of Electrical and Electronics Engineers,** volume 57, number 11, pages 2071 – 2072, November 1969.

4. A. H. Nuttall, "Numerical Evaluation of Cumulative Probability Distribution Functions Directly from Characteristic Functions," NUSL Report Number 1032, Naval Underwater Systems Center, New London, CT, 11 August 1969.

APPENDIX A — BASIC PROGRAM FOR PDF

```
10   ! SMALL TAIL PROBABILITIES        "CHI-SQUARE-PDF"
20     R=.7                        ! AMOUNT OF CONTOUR SHIFT USED
30     Dx=2.*PI/240.               ! SAMPLING INCREMENT IN X
40     C=0.                        ! ADDITIVE CONSTANT
50     N=1024                      ! SIZE OF FFT
60     Y1=-90.                     ! LOWER LIMIT OF LGT RANGE
70     Y2=0.                       ! UPPER LIMIT OF LGT RANGE
80     Tol=1.E-36                  ! TOLERANCE ON MAG SQ CHAR FN
90     N1=N-1
100    REDIM Cos(0:N/4),X(0:N1),Y(0:N1)
110    DIM Cos(4096),X(16384),Y(16384)
120    DOUBLE N,N1,K,M,Ns          ! INTEGERS, NOT DOUBLE PRECISION
130    A=2.*PI/N
140    FOR K=0 TO N/4
150    Cos(K)=COS(A*K)             ! QUARTER-COSINE TABLE IN Cos(*)
160    NEXT K
170      A1=10.                    ! CF f(xi) = 1/(1 - i xi)^alpha
180      R1=1.-R
190      F0=1./R1^A1
200      X(0)=.5
210      Y(0)=0.
220      M=0
230      M=M+1
240      X=Dx*M
250      CALL Power(R1,-X,-A1,Ar,Ai)
260      Fr=Ar/F0                  ! REAL CF
270      Fi=Ai/F0                  ! IMAG CF
280      K=M MODULO N              ! PREALIASING
290      X(K)=X(K)+Fr
300      Y(K)=Y(K)+Fi
310      IF (Fr*Fr+Fi*Fi>Tol) THEN 230
320    CALL Fft14(N,Cos(*),X(*),Y(*))
330      MAT X=X*(Dx/PI)
340      Big=MAX(X(*))
350      GINIT
360      PLOTTER IS "GRAPHICS"
370      GRAPHICS ON
380      WINDOW 0,N,-18,0
390      LINE TYPE 3
400      GRID N/8,2
410      LINE TYPE 1
420      FOR Ns=0 TO N1
430      Pn=X(Ns)                  ! PDF TILDA
440      IF Pn<>0. THEN 470
450      PENUP
460      GOTO 480
470      PLOT Ns,LGT(ABS(Pn)/Big)  ! NORMALIZED PDF TILDA
480      NEXT Ns
490      PENUP
500      PAUSE
```

```
510        Du=2.*PI/(N*Dx)                ! U INCREMENT
520        FOR Ns=0 TO N1
530        U=Du*Ns
540        X(Ns)=F0*EXP(-R*U)*X(Ns)       ! PDF ESTIMATE
550        NEXT Ns
560        GCLEAR
570        WINDOW 0,N,Y1,Y2
580        LINE TYPE 3
590        GRID N/8,10
600        A1=A1-1.
610        Ga=FNGamma(A1)
620        FOR Ns=1 TO N STEP 10
630        U=Du*Ns
640        Pe=FNEx(U-A1*LOG(U))/Ga        ! PDF EXACT
650        PLOT Ns,LGT(Pe)
660        NEXT Ns
670        PENUP
680        PAUSE
690        LINE TYPE 1
700        FOR Ns=0 TO N1
710        Pn=X(Ns)                       ! PDF ESTIMATE
720        IF Pn<>0. THEN 750
730        PENUP
740        GOTO 760
750        PLOT Ns,LGT(ABS(Pn))
760        NEXT Ns
770        LINE TYPE 3
780        MOVE 0,LGT(ABS(X(0)))          ! ERROR
790        DRAW N1,LGT(ABS(X(N1)))        ! ESTIMATE
800        PENUP
810        PAUSE
820      END
830        !
840      DEF FNEx(X)                      ! EXP(-X)
850      IF X>708. THEN RETURN 0.
860      RETURN EXP(-X)
870      FNEND
880        !
890      SUB Power(X,Y,Real,U,V)          ! PRINCIPAL POWER Z^Real
900      T=X*X+Y*Y
910      IF T>0. THEN 950
920      U=V=0.
930      IF Real=0. THEN U=1.
940      SUBEXIT
950      F=EXP(.5*Real*LOG(T))
960      IF X=0. THEN A=.5*PI*SGN(Y)
970      IF X<>0. THEN A=ATN(Y/X)
980      IF X<0. THEN A=A+PI*(1.-2.*(Y<0.))
990      T=Real*A
1000     U=F*COS(T)
1010     V=F*SIN(T)
1020     SUBEND
1030       !
1040     DEF FNGamma(X)                   !   HART, page 135, #5243
1370       !
1380     SUB Fft14(DOUBLE N,REAL Cos(*),X(*),Y(*)) ! N<=2^14=16384; 0 SUBS
```

APPENDIX B — BASIC PROGRAM FOR EDF

```
10   ! SMALL TAIL PROBABILITIES           "CHI-SQUARE-EDF"
20     Dx=2.*PI/240.              !  SAMPLING INCREMENT IN X
30     R=.6                       !  AMOUNT OF CONTOUR SHIFT USED
40     N=1024                     !  SIZE OF FFT
50     Y1=-70.                    !  LOWER LIMIT OF LGT RANGE
60     Y2=10.                     !  UPPER LIMIT OF LGT RANGE
70     Tol=1.E-30                 !  TOLERANCE ON MAG SQ CHAR FN
80     N1=N-1
90     REDIM Cos(0:N/4),X(0:N1),Y(0:N1)
100    DIM Cos(4096),X(16384),Y(16384)
110    DOUBLE N,N1,K,M,Ns,Nf  !  INTEGERS, NOT DOUBLE PRECISION
120    A=2.*PI/N
130    FOR K=0 TO N/4
140    Cos(K)=COS(A*K)            !  QUARTER-COSINE TABLE IN Cos(*)
150    NEXT K
160      MAT X=(0.)
170      MAT Y=(0.)
180      A1=10.                   !  CF f(xi) = 1/(1 - i xi)^alpha
190      R1=1.-R
200      R2=R*R
210      X(0)=.5/(R1^A1*R)
220      M=0
230      M=M+1
240      X=Dx*M
250      CALL Power(R1,-X,-A1,Ar,Ai)
260      A=R2+X*X
270      Fr=(Ar*R+Ai*X)/A    !  REAL CF
280      Fi=(Ai*R-Ar*X)/A    !  IMAG CF
290      K=M MODULO N        !  PREALIASING
300      X(K)=X(K)+Fr
310      Y(K)=Y(K)+Fi
320      IF (Fr*Fr+Fi*Fi)>Tol THEN 230
330    CALL Fft14(N,Cos(*),X(*),Y(*))
340      MAT X=X*(Dx/PI)
350      Big=MAX(X(*))
360      GINIT
370      PLOTTER IS "GRAPHICS"
380      GRAPHICS ON
390      WINDOW 0,N,-18,0
400      LINE TYPE 3
410      GRID N/8,2
420      LINE TYPE 1
430      FOR Ns=0 TO N1
440      En=X(Ns)                 !  EDF TILDA
450      IF En<>0. THEN 480
460      PENUP
470      GOTO 490
480      PLOT Ns,LGT(ABS(En)/Big)  !  NORMALIZED EDF TILDA
490      NEXT Ns
500      PENUP
```

```
510        INPUT "INPUT FRACTION OF PERIOD",Frac
520        Nf=N*Frac
530        Du=2.*PI/(N*Dx)                ! U INCREMENT
540        FOR Ns=0 TO Nf
550        U=Du*Ns
560        X(Ns)=EXP(-R*U)*X(Ns)          ! EDF E(u)
570        NEXT Ns
580        Rp=R*2.*PI/Dx
590        FOR Ns=Nf+1 TO N1
600        U=Du*Ns
610        X(Ns)=EXP(-R*U+Rp)*X(Ns)   ! EDF E(u)
620        NEXT Ns
630        GCLEAR
640        WINDOW 0,N,Y1,Y2
650        LINE TYPE 3
660        GRID N/8,10
670        A1=A1-1.
680        Ga=FNGamma(A1)
690        FOR Ns=0 TO N STEP 10
700        U=Du*Ns
710        S=T=1.
720        FOR K=1 TO A1
730        T=T*U/K
740        S=S+T
750        NEXT K
760        Ee=EXP(-U)*S              ! EDF EXACT
770        IF Ee>0. THEN 800
780        PENUP
790        GOTO 810
800        PLOT Ns,LGT(Ee)
810        NEXT Ns
820        PENUP
830        LINE TYPE 1
840        FOR Ns=0 TO N1
850        En=X(Ns)                  !   ESTIMATED EDF
860        IF En<>0. THEN 890
870        PENUP
880      -  GOTO 900
890        PLOT Ns,LGT(ABS(En))
900        NEXT Ns
910        PENUP
920        PAUSE
930        GRAPHICS OFF
940     END
950        !
960     SUB Power(X,Y,Real,U,V)  !  PRINCIPAL POWER Z^Real
1100       !
1110    DEF FNGamma(X)          !   HART, page 135, #5243
1440       !
1450    SUB Fft14(DOUBLE N,REAL Cos(*),X(*),Y(*)) ! N<=2^14=16384; 0 SUBS
```

INITIAL DISTRIBUTION LIST

Addressee	No. of Copies
Center for Naval Analyses, VA	1
Coast Guard Academy, CT	
J. Wolcin	1
Defense Technical Information Center, VA	12
Griffiss Air Force Base, NY	
Documents Library	1
J. Michels	1
Hanscom Air Force Base, MA	
M. Rangaswamy	1
National Radio Astronomy Observatory, VA	
F. Schwab	1
National Security Agency, MD	
J. Maar	1
National Technical Information Service, VA	10
Naval Air Warfare Center, PA	
L. Allen	1
Naval Command Control and Ocean Surveillance Center, CA	
J. Alsup	1
W. Marsh	1
P. Nachtigall	1
C. Tran	1
Naval Environmental Prediction Research Facility, CA	1
Naval Intelligence Command, DC	1
Naval Oceanographic and Atmospheric Research Laboratory, CA	
M. Pastore	1
Naval Oceanographic and Atmospheric Research Laboratory, MS	
B. Adams	1
R. Fiddler	1
E. Franchi	1
R. Wagstaff	1
Naval Oceanographic Office, MS	1
Naval Personnel Research and Development Center, CA	1
Naval Postgraduate School, CA	
Superintendent	1
C. Therrien	1
Naval Research Laboratory, DC	
W. Gabriel	1
D. Steiger	1
E. Wald	1
N. Yen	1
Naval Surface Warfare Center, FL	
E. Linsenmeyer	1
D. Skinner	1
Naval Surface Warfare Center, MD	
P. Prendergast	1

Addressee	No. of Copies
Naval Surface Warfare Center, VA	
J. Gray	1
Naval Technical Intelligence Center, DC	
Commanding Officer	1
D. Rothenberger	1
Naval Undersea Warfare Center, FL	
Officer in Charge	1
Naval Weapons Center, CA	1
Office of the Chief of Naval Research, VA	
P. Abraham	1
N. Gerr	1
N. Harned	1
D. Johnson	1
R. Tipper	1
A. van Tilborg	1
Space and Naval Warfare Systems Command, DC	
R. Holland	1
U.S. Air Force, Maxwell Air Force Base, AL	
Air University Library	1
U.S. Department of Commerce, CO	
A. Spaulding	1
Vandenberg Air Force Base, CA	
R. Leonard	1

Addressee	No. of Copies
Brown University, RI	
Documents Library	1
Catholic University, DC	
J. McCoy	1
Drexel University, PA	
S. Kesler	1
Duke University, NC	
J. Krolik	1
Harvard University, MA	
Gordon McKay Library	1
Lawrence Livermore National Laboratory, CA	
L. Ng	1
Los Alamos National Laboratory, NM	1
Marine Biological Laboratory, MA	1
Massachusetts Institute of Technology, MA	
Barker Engineering Library	1
Northeastern University, MA	
C. Nikias	1
Pennsylvania State University, PA	
R. Hettche	1
E. Liszka	1
F. Symons	1
Princeton University, NJ	
S. Schwartz	1
Rutgers University, NJ	
S. Orfanidis	1
San Diego State University, CA	
F. Harris	1
Sandia National Laboratory, NM	
J. Claasen	1
Scripps Institution of Oceonography, CA	1
Syracuse University, NY	
D. Weiner	1
United Engineering Center, NY	
Engineering Societies Library	1
University of Colorado, CO	
L. Scharf	1
University of Connecticut, CT	
Wilbur Cross Library	1
C. Knapp	1
P. Willett	1
University of Florida, FL	
D. Childers	1
University of Hartford	
Science and Engineering Library	1
University of Illinois, IL	
D. Jones	1
A. Nehorai	1

Addressee	No. of Copies
University of Massachusetts Dartmouth, MA	
C. Chen	1
University of Michigan, MI	
Communications and Signal Processing Laboratory	1
W. Williams	1
University of Minnesota, MN	
M. Kaveh	1
University of Rhode Island, RI	
Library	1
G. Boudreaux-Bartels	1
S. Kay	1
D. Tufts	1
University of Rochester, NY	
E. Titlebaum	1
University of Southern California, CA	
W. Lindsey	1
A. Polydoros	1
University of Texas, TX	1
University of Washington, WA	
Applied Physics Laboratory	1
D. Lytle	1
J. Ritcey	1
R. Spindel	1
Villanova University, PA	
M. Amin	1
Woods Hole Oceanographic Institution, MA	
Director	1
T. Stanton	1
Yale University, CT	
Kline Science Library	1
P. Schultheiss	1

Addressee	No. of Copies
Analysis and Technology, CT	
Library	1
Analysis and Technology, VA	
D. Clark	1
Atlantic Aerospace Electronics Corporation	
R. Stahl	1
Bell Communications Research, NJ	
D. Sunday	1
Berkeley Research, CA	
S. McDonald	1
Bolt, Beranek, and Newman, CT	
P. Cable	1
Bolt, Beranek, and Newman, MA	
H. Gish	1
EDO Corporation, NY	
M. Blanchard	1
E G & G, VA	
D. Frohman	1
Engineering Technology Center	
D. Lerro	1
General Electric, MA	
R. Race	1
General Electric, NJ	
H. Urkowitz	1
Harris Scientific Services, NY	
B. Harris	1
Hughes Defense Communications, IN	
R. Kenefic	1
Hughes Aircraft, CA	
T. Posch	1
Kildare Corporation, CT	
R. Mellen	1
Lincom Corporation, MA	
T. Schonhoff	1
MITRE Corporation, CT	
S. Pawlukiewicz	1
Orincon Corporation, CA	
J. Young	1
Orincon Corporation, VA	
H. Cox	1
Prometheus, RI	
M. Barrett	1
J. Byrnes	1
Raytheon Company, RI	
R. Conner	1
S. Reese	1
Schlumberger-Doll Research, CT	
R. Shenoy	1

Addressee	No. of Copies

Scientific Applications International Corporation, CA
    C. Katz   1
Scientific Applications International Corporation, VA
    P. Mikhalevsky   1
Toyon Research, CA
    M. Van Blaricum   1
Tracor, TX
    T. Leih   1
    B. Jones   1
    K. Scarbrough   1
TRW, VA
    R. Prager   1
    G. Maher   1
Westinghouse Electric, MA
    R. Kennedy   1
Westinghouse Electric, MD
    H. Newman   1
Westinghouse Electric, MD
    R. Park   1